Elemental distributions and mineral parageneses of the Skaergaard PGE-Au mineralisation: consequences of accumulation, redistribution, and equilibration in an upward-migrating mush zone

Journal:	*Journal of Petrology*
Manuscript ID	JPET-Mar-18-0036.R2
Manuscript Type:	Original Manuscript
Date Submitted by the Author:	n/a
Complete List of Authors:	Nielsen, Troels; Geological Survey of Denmark and Greenland, Department of Petrology and Economic Geology Rudashevsky, Nikolay; CNT Instruments LLC Rudashevsky, Vladimir; CNT Instruments LLC Weatherley, Samuel; Geological Survey of Denmark and Greenland, Department of Petrology and Economic Geology; Teck Resources Limited Andersen, Jens; University of Exeter, Camborne School of Mines
Keyword:	Skaergaard, PGE-Au, mush melts, gabbro, magma chamber

Elemental distributions and mineral parageneses of the Skaergaard PGE-Au mineralisation: consequences of accumulation, redistribution, and equilibration in an upward-migrating mush zone

T F.D. Nielsen[1*], N.S.Rudashevsky[2], V.N. Rudashevsky[2], S. M. Weatherley[1,4] and J. C.Ø Andersen[3]

[1]Department of Petrology and Economic Geology, Geological Survey of Denmark and Greenland, Øster Voldgade 10, 1350 Copenhagen Denmark

[2]CNT Instruments LLC, Svetlanovskiy Ave. 75-41, 195427, St. Petersburg, Russia

[3]Camborne School of Mines, College of Engineering, Mathematics and Physical Sciences, University of Exeter, Penryn, Cornwall TR10 9FE, UK

[4] Present address: Teck Resources Limited, Suite 3300, Bentall 5, 550 Burrard Street, Vancouver, B.C. V6C 0B3, Canada.

*Corresponding author: Telephone +4591333886; Fax: +45 38142050. E-mail: tfn@geus.dk

Abstract

The Skaergaard PGE-Au mineralisation, alias the Platinova Reef, is syn-magmatic Platinum Group Element (PGE) and gold (Au) mineralisation that formed after crystallisation of ~74% of the bulk melt of the intrusion. It is hosted in a more than 600 m deep and bowl-shaped succession of gabbroic macro-rhythmic layers in the upper 100 m of Middle Zone. The precious metal mineralisation comprises a series of concordant but compositionally zoned mineralisation levels identified by distinct PGE, Au and Cu peaks. They formed due to local sulphide saturation in stratiform concentrations of interstitial and evolved mush melts in six MLs over > 2000 years. The PGE-Au mineralisation is compared to a stack of gold-rimmed saucers of PGE-rich gabbro of upward decreasing size. Fundamentally different crystallisation and mineralisation scenarios have been proposed for the mineralisation, including offset reef type models based on sulphide saturation in the melt from which the silicate host crystallised, and the here argued model which restricts the same processes to the melt of the inward migrating mush zone of the magma chamber. The latter is supported by: i) a 3D summary of the parageneses of precious metal minerals and phases (> 4000 grains) from 32 samples across the mineralisation; ii) a 3D compilation of all bulk rock assay data; and iii) a principal component analysis (PCA) on PGE, Au, Cu, and selected major-and trace elements. In the main PGE-mineralisation level (Pd5 alias Pd-Zone) the precious metal mineral paragenesis varies across the intrusion with precious metal sulphides and Au-alloys at the W-margin to Precambrian basement, precious metal plumbide and Au- and Ag alloys at the E-margin to flood basalts, and skaergaardite (PdCu) and intermetallic compounds and alloys of PGE-Au and Cu in the central parts of the mineralisation. Precious metal parageneses are distinct for a given sector of the intrusion i.e., drill core (local control), rather than for a given stratigraphic or temporal interval in the accumulated gabbros. The precious metal "grade times width" number (average g/t x metres) for the mineralisation at

an upper and a lower cut off of 100 ppb PGE or Au increases from ~20 to ~45 g toward the centre of the mineralisation due to ponding of precious metal bearing melt. A strong increase in (Pd+Pt+Au)/Cu and dominance of (PdCu) alloys in the lower and central parts of the mineralisation demonstrate the partial dissolution of droplets of Cu-rich sulphide melt and fractionation of precious metal ratios. The precious metal parageneses, the distribution of precious metals in the mineralisation, and the PCA support initial accumulation of precious metals in melt of the mush in the floor followed by equilibration, sulphide saturation, and reactions with residual and immiscible Fe-rich silicate melt in a series of macro-rhythmic layers in the stratified and upward migrating mush zone in the floor of the magma chamber. Syn-magmatic and upward redistribution of precious metals sets the Skaergaard PGE-Au Mineralisation apart from conventional reef type and offset-reef type precious metal mineralisations and characterize "Skaergaard type" precious metal deposits.

Introduction

The Skaergaard PGE-Au mineralisation (Nielsen *et al.*, 2015), also referred to as the Platinova Reef (Andersen *et al.*, 1998), is a large, low grade Platinum Group Element (PGE) and gold (Au) mineralisation hosted in the upper 100 m of Middle Zone gabbros of the intrusion (Fig. 1). The mineralisation is estimated to have an inferred s resource of >30 million ounces (oz.) PGE and ~9 million oz. Au (Kuo, 2007; Nielsen *et al.*, 2005) and approximates giant mineralisations as defined by Laznicka (2006). It relates to stratiform precious metal mineralisation in layered mafic intrusions for which models range from contamination-, magma mixing- or fractionation-driven sulphide saturation leading to gravitational accumulation of droplets of immiscible sulphide melt, to upwards-directed transportation of precious metals in

residual melts or fluids and re-deposition, for example at redox barriers, to form precious metal reefs (e.g., review in Barnes *et al.*, 2017; Boudreau, 2004; Boudreau & Meurer, 1999).

Mineralisation models based on in sulphide saturation currently provide the most plausible explanation for of the Skaergaard PGE-Au mineralisation. Within this class, there are currently two different models, outlined most recently by Nielsen *et al.* (2015) and Holwell *et al.* (2016) that described the structure of the mineralisation and the processes inherent in its formation. They are based on contrasting perceptions of the structure of the mineralisation and the distribution of precious metals in the layered gabbros. Nielsen *et al.* (2015) model the mineralisation as a suite of concordant but compositionally zoned mineralisation levels within a >600m deep bowl in the floor of the intrusion, whereas Holwell & Keays (2014) build on correlation of precious metals anomalies, with increasing number of mineralisation levels in the geographic centre of the mineralisation (hereafter "centre") and a capping gold-zone. In the centre of the mineralisation the Au-zone of Holwell & Keays (2014) is above leucograbbro layer 2 (L2) and at the margin of the intrusion below leucograbbro layer 1 (L1) of the Triple Group, some 40 meters lower in the succession of gabbroic layers.

Nielsen et al. (2015) and Holwell *et al.* (2016) argue for accumulation of immiscible droplets of sulphide melt enriched in precious metals that were subsequently subjected to reaction with Fe-rich silicate melt. Constrained by their perceptions of the structure of the mineralisation Holwell & Keays (2014) and Holwell *et al.* (2015, 2016) suggested that sulphide droplets to sank through and scavenged precious metals from the bulk liquid accumulated and partly dissolved in Fe-rich silicate melt that ponded at the crystallisation front at the floor of the magma chamber. The elemental variations up the gabbroic layers of the mineralisation would therefore in modified form reflect fractionation and evolution of bulk

liquid. The model is based and supported by observations mainly from drill cores from near the margin of the intrusion (e.g., Holwell *et al.*, 2016).

Nielsen et al. (2015) alternatively argued the bulk melt was circulated into the crystallisation zone under the roof of the magma chamber, where it fractionated, reached sulphide saturation, and subsequently immiscibility between Fe- and Si-rich silicate melts. The tiny Cu-rich sulphide droplets that formed at sulphide saturation, had a density similar to FeTi-oxides and were suspended in the mush melt. When the mush melt reached the two-liquid field between Fe- and Si rich silicate liquids and buoyant Si-rich melt rose, the already formed Cu-rich sulphide droplets dissolved into the dense and Fe-rich conjugate that descended along the walls to the floor of the magma chamber. Next, the now dissolved precious metals were re-deposited in macro-rhythmic layers during upward migration of the mushy crystallisation zone in the floor of the intrusion. In each macro-rhythmic layers the processes were repeated: i) crystal fractionation; ii) density controlled concentration of mush melt; iii) sulphide saturation and trapping of precious metals; iv) liquid immiscibility and loss of Si-rich conjugate; v) reaction and dissolution of sulphide droplets leaving behind precious metal phases in the gabbros. It is a model that combines initial accumulation followed by an upward redistribution of precious metals in the mineralisation. The main difference between the proposed sulphide saturation type models are not the processes involved (sulphide saturation, dissolution and fractionation in accordance with partition coefficients), but the timing of mineralisation processes relative to the crystallisation of the host rocks, and the volumes of melt to which the processes are applied.

Lateral variations are significant in the intrusion and no single drill core can be representative for the mineralisation. In this contribution we illustrate the 3D distributions of the precious metals and their mineral parageneses in a search for additional constraints for the

proposed mineralisation models. Specifically, we compiled the information in order to evaluate the validity of the two-stage model and the upward redistribution of the precious metals in the mineralisation (Nielsen *et al.*, 2015). We include: (i) as a basis for the evaluations of the proposed models, a summary of the fundamental elemental distributions and structural observations that are critical for the perception of the structure of Skaergaard-type mineralisations and the relative timing of processes in the intrusion, (ii) intrusion-wide compilation and interpretation of the precious metal mineral parageneses from 32 samples from drill cores and bulk samples (the mineralogical data for individual samples were collected 2003-2012 but have not been compiled and discussed in any detail prior to this work), (iii) the distribution of precious metal in the mineralisation using here compiled grade*width numbers (g*w; average g/t times width or height in metres) compiled for stratigraphic intervals on basis of systematic bulk rock assays (Watts, Griffis and McOuat, 1990; Hanghøj, 2005), and (iv) a principal component analysis (PCA) of the distribution of precious metals, incompatible elements and major element oxides in the fully developed mineralisation in the centre of the mineralisation. The PCA is carried out to confirm combination of processes proposed to be responsible for the distribution of the precious metals. Supplementary information, including elemental correlations, paragenetic information, additional chemical information, and details on the PC analysis are provided in electronic appendices EA1 to EA14 attached to this work.

The Skaergaard intrusion

The Skaergaard intrusion is 56 Ma (Wotzlaw *et al.*, 2012) and was emplaced during the opening of the North Atlantic. It is a comparatively small, but well-preserved and well-exposed layered gabbro intrusion (Fig. 1a,). It is ~7 x 11 km in surface size (Wager & Brown, 1968), ~4 km in thickness, and has a box-like or ellipsoidal shape with a volume of ~300 km^3 (Irvine *et al.*, 1998;

Nielsen, 2004; Svennevig & Guarnieri, 2012). The magma crystallised inwards in an onion-ring type structure (Fig. 1b) with the Layered Series including Hidden Zone (HZ), Lower Zone (LZ), Middle Zone (MZ) and Upper Zone (UZ) in the bowl-shaped floor, the Marginal Border Series (MBS) along the walls, and the Upper Border Series (UBS) below the roof. The UBS and LS meet at the Sandwich horizon (SH) (Figs 1b and c) in the upper and central part of the intrusion. All three series are further subdivided on basis of their parallel evolution of liquidus parageneses (Wager & Brown, 1968; Salmonsen &Tegner, 2013 and references therein; see Fig. 1). Significant volumes of melanogranophyre and granophyre occur as sill-like bodies in and between SH and UBS gabbros and represent strongly evolved compositions on the line of liquid descent (Wager & Brown, 1968; McBirney, 1989; Nielsen 2004; Salmonsen, 2013). Detailed accounts of the intrusion are found in Wager & Brown (1968), McBirney (1996), Irvine *et al.* (1998), and Nielsen (2004).

The mineralisation

The following description of the Skaergaard PGE-Au mineralisation is a summary based on Nielsen (2004) and Nielsen *et al.* (2015), who identified and correlated elemental, lithological and density anomalies between forty-one drill cores and additional chip lines from the intrusion. N-S and E-W correlations between drill cores are provided in Andersen *et al.* (1998), Nielsen *et al.* (2015), and Holwell & Keays (2014). All publicly available primary information, including the correlation between systematic assays and lithological logs in the drill cores, and density logs (which are proxies for lithology) from thirteen drill cores are included in Nielsen *et al.* (2015, references therein, and SD1-SD3, and SD5 of that publication) and EA1-EA4 of the present work.

In its centre the mineralisation is hosted in the lower ~60 m of the Triple Group (TG, Fig. 2a; Andersen *et al.*, 1998; Holness *et al.*, 2017c). Triple Group is a ~100 m thick, bowl-shaped succession of macro-rhythmic layers (MLs) located in the uppermost part of Middle Zone, in the Layered Series in the floor of the intrusion (Nielsen, 2004). TG owes its name to three prominent leucogabbro layers referred to as L1, L2 and L3, which are easily observed from a distance (Fig. 2a and b). These leucogabbro layers are lithological markers that provide constraints on the relative timing of the accumulation of the gabbroic host and the precious metals. Nielsen (2004) modelled the structure of the Layered Series in 2D in E-W and N-S sections, and Nielsen *et al.* (2009) extended the models to three dimensions using the geological modelling tool Leapfrog®. These models constrain the bowl-shaped layering in the Layered Series to be ~7000 m wide (E-W) and >600 m deep (Fig. 3; Nielsen *et al.*, 2015; Holness *et al.*, 2017b). The distribution of precious metals is roughly concentric and the mineralisation fully developed around a centre in the south-central part of the intrusion where MZ is at its thickest (Watts, Griffis and McOuat, 1991; Andersen *et al.*, 1998; Nielsen, 2004; Nielsen *et al.*, 2005, 2015).

The fully developed precious metal mineralisation

The fully developed PGE-rich part of the mineralisation is in its centre hosted in eight stratigraphic intervals of host gabbro. The mineralised intervals of gabbro are referred to as Pd-levels (Fig. 3a,) and each interval has upward decreasing Pd/Pt and an easily identified Pd-dominated peak (Nielsen *et al.*, 2005, 2015). The Pd-levels and peaks are numbered top-down from Pd1 to Pd6 and with sub-fixes *'a'* and *'b'* for levels Pd2-Pd4 (Nielsen *et al.*, 2005). Individual Pd-levels can be correlated across the intrusion (Fig. 3a, EA1). The naming of the Pd-levels is a reminiscence of the earliest identification of mineralisation levels in early years of

exploration (1986-1990). The main resource of PGEs is in level Pd5. In this work, the peak concentration of PGE (Pd+Pt) in the Pd5 is used as marker and for all correlations between drill core logs and systematic assays.

Au/PGE increases up the mineralisation (Andersen *et al.*, 1998; Nielsen *et al.*, 2005; Holwell & Keays, 2014). Above Pd1, a PGE-poor but Au-rich stratigraphic intervals identifies the top of the succession of gabbros enriched in precious metals. It is elevated ~2 m above Pd1 and is referred to as Au/Pd1 (see, e.g., drill core 90-22 in Fig. 3a). Overlying Cu-bearing intervals with 100-200 ppb gold are numbered sequentially with increasing height from Au+1, Au+2 etc. Au+1 is located ~13 m above Au/Pd1 (see, e.g., drill core 89-09 in Andersen *et al.*, 1998) and is identified in more drill cores despite very low levels of Au.

All Pd-levels maintain near-constant elevations relative to Pd5 and can be correlated across the intrusion at the exact same stratigraphic position, irrespectively of the absolute concentration of precious metals or Cu (Fig. 3a, Table 1, EA1). For example, the double peaks Pd2a and b, and Pd3a and b, can be identified near the margins of the intrusion even at very low (10-100 ppb) bulk concentrations (Fig. 3a, EA2). Pd-levels are stratigraphic intervals of gabbroic host *with or without* precious metal concentrations. The concentrations and elemental ratios of precious metals and Cu vary laterally in the Pd-levels. For example, peak Pd2b is PGE-rich in the centre of the mineralisation (Fig. 3a, drill core 90-22), Au-rich approximately half way between the centre and margin of the concentric mineralisation (Fig. 3a, drill core 90-17A) and Cu-rich near the margin (Fig. 3a, drill core 90-23A). In no case is the main gold-rich peak detached from a mineralisation level that can be identified across the intrusion at the given stratigraphic level in the succession of macro-rhythmic layers.

Correlation to the gabbroic host and the saucer model

Systematic structural relationships are observed between mineralised levels and the host gabbros of the intrusion. For example, the peak concentration of PGE in Pd5 is always located ~2 meters below the top of leucogabbro layer L0 (defined as the leucogabbro top to the lowermost ML in the mineralised interval, see SD5 in Nielsen et al., 2015) and Pd1 is always ~40 m above Pd5, ~3 m above the top of the L2 leucogabbro member of the Triple Group, irrespectively of the absolute concentration of precious metals (Fig. 3a, Table 1; see also Andersen et *al.*, 1998; and SD1, and SD3 in Nielsen *et al.*, 2015)). The near-constant stratigraphic separations between Pd-levels observed in all available drill cores, and the correlation between 13 density profiles aligned at the Pd5 peak (EA3), highlight that the mineralisation levels are concordant with the host rocks across the bowl-shaped floor of the intrusion (Table 1). The elevations relative to sea level of Pd5 and Pd1 peaks and leucogabbro layer L3 in drill cores are traced across the intrusion (Fig. 3b) and illustrate the concordant relationship between leucogabbro layers and Pd-levels in the >600 meter deep bowl of Triple Group (Fig. 3b).

The stratigraphic separation between Pd5 to the main Au-peak decreases from >43 m at the central parts of the mineralisation to < 1 m in the most distant profiles (Fig. 3a). In the Midnat and Middag Buttress chip lines located farthest away from the centre of the mineralisation (Fig. 1a), the PGE and peak concentrations of Au overlap within the same metre of gabbro (Andersen *et al.*, 1998; Turner & Mosher, 1989). The distribution of precious metals in the intrusion is therefore diachronous relative to the layering in the gabbroic host (Fig. 3a) and no single drill core can provide representative assays through the Skaergaard PGE-Au mineralisation. Some represent the fully developed succession of gabbroic MLs in the centre of the mineralisation (e.g., 90-22; Bernstein & Nielsen, 2004), some the little-developed mineralisation at the margins (e.g., EA2; Holwell *et al*., 2016), whilst the remainder are transitional between the two.

The integration of the of the bowl-shape of the layered gabbros (Figs 1b and 3b), the concordant Pd-levels, and the variation in concentration of precious metals through the ML stratigraphy (Fig. 3a; SD3 in Nielsen *et al.*, 2015) resulted in the mineralisation being described as a succession of gold-rimmed saucers of PGE-enriched gabbro that decrease in diameter up through the stratigraphy (Fig. 4).

Macro-rhythmic layers and compositional subdivision

Density (ρ) logs can be used as a proxy for lithology, and correlations across the intrusion. Leucogabbro layers are easily followed as concordant stratigraphic intervals (EA3; see also Nielsen *et al.*, 2015). The following division of the host rock lithology in drill core 90-22 (Bernstein & Nielsen, 2004; Tegner *et al.*, 2009; Nielsen et al., 2015) therefore applies to the host gabbros across the intrusion. This drill core was chosen out of eleven from central parts of the mineralisation for the establishment of the so-called 'Standard Profile' in the Skaergaard intrusion (Nielsen *et al.*, 2000; Tegner *et al.*, 2009; Keays & Tegner, 2016) because it has a very high recovery with very few intersecting dikes within the mineralised interval (Tegner *et al.*, 2009).

The gabbros of the Triple Group divide into several MLs that encapsulate the prominent leucogabbro layers shown in Fig. 2. The MLs have dense, pyroxene-rich bases (ρ = 3.4-3.6 g/cm^3; modal abundance of plagioclase relative to clinopyroxene ≅0.5) and low density and plagioclase-rich tops (ρ =2.9-3.1 g/cm^3; modal abundance of plagioclase relative to clinopyroxene >2) (data in Bernstein & Nielsen, 2004; Nielsen *et al.*, 2015). Transitions between MLs are located immediately above the leucogabbro layers, in sections of gabbro with a marked upward increase in the proportion of clinopyroxene relative to plagioclase, and an accompanying increase in density. Nielsen *et al.* (2015) divided the stratigraphic interval enriched in precious

metals in drill core 90-22 into four MLs including ML0, ML1, ML2 and ML2.1 (named with reference to the included leucogabbro layers L0, L1 and L2), where ML0 is the lowest-most ML.

In this study, the lithological sub-division of the stratigraphic interval of the mineralisation is revised to comprise six ML layers that each maintain near constant stratigraphic thickness across the intrusion. ML1 of Nielsen *et al.* (2015) was exceptionally thick (>20 versus ~13 m for all other MLs) and, based on re-evaluation of the density logs, it is now divided into ML1.1, ML1.2, and ML2.2 is added above ML2.1. Low-density layers in the tops of ML1.1 (~10 m above Pd5 marker) and ML2.1 (~50 m above Pd5 marker) are easily followed across the intrusion in the density logs (EA3). Table 1 and Fig. 5 outline the revised lithological subdivision of the gabbroic host of the mineralisation. ML0 hosts precious metal mineralisation levels Pd6 and Pd5 (Subzone and Pd-zone of Holwell & Keays, 2014), ML1.1 hosts Pd4a and b, ML1.2 host Pd-levels Pd3a and b, ML2 hosts Pd2a and b, ML2.1 hosts Pd1 and Au/Pd1, and ML2.2 hosts the Au+1 (Fig. 5).

Each ML includes a lower precious metal level which Nielsen *et al.* (2015) argue is cumulative and an upper level in mush melt accumulated in the base of the low density roof of the MLs (Fig. 5). In Figure 5 is included sections of drill core 90-22 enriched in tiny euhedral crystals of ilmenite that cannot sink. These layers are found in all lithologies including leuco-, meso-, and melanograbbros and show no relationship to mineralisation levels or to the distribution of precious metals and Cu. They are in Nielsen *et al.* (2015) understood as formed due to stratbound nucleation of ilmenite in the melt of the stratified mush zone.

In addition to the lithologic sub-division into MLs, Nielsen *et al.* (2015) sub-divided the fully developed mineralisation on the basis of the distribution of the precious metals. The fully developed mineralisation (e.g. in drill core 90-22) was divided into the "Lower PGE Mineralisation" (LPGEM) comprising ML0 and ML1.1 (Pd6, Pd5, Pd4a and b levels), and the

"Upper PGE Mineralisation" (UPGEM) comprising ML1.2, ML2, ML2.1 (Pd3a and b, Pd2a and b, Pd1 and Au/Pd1 levels, see Fig. 5). LPGEM is rich in precious metals across the floor, whereas in the UPGEM, the precious metals are increasingly restricted to smaller and smaller gold-rimmed bowls upwards through the sequence of MLs and towards the centre of the mineralisation (Figs 4-5).

Au/PGE in bulk samples increases upwards through the mineralisation levels (Bird *et al.*, 1991; Andersen *et al.*, 1998). Skaergaardite (PdCu) is the main precious metal phase in lower mineralisation levels in the central parts of the mineralisation. It is increasingly Au-rich up through the mineralisation levels and is in the upper parts of the mineralisation accompanied by tetra-auricupride (AuCu) (Nielsen *et al*., 2005; Rudashevsky *et al.*, 2014). In addition, Au also occurs as anhedral grains on grain boundaries in already crystallised gabbros (Godel *et al.*, 2014; Rudashevsky *et al.*, 2014). This additional form of gold deposition is referred to as the "Upper Au Mineralisation" (UAuM) (Nielsen *et al.*, 2015) and is observed in or above the upper most Pd-level with more than traces of PGE (Fig. 6). The upward distribution of Au in the top of the precious metal rich mineralisation is illustrated by drill core 89-09 (Turner & Mosher, 1990). The core was drilled near the centre of the mineralisation and ~1.5 km NW of drill core 90-22. It was wedged twice and the three parallel drill cores have very similar (g*w) numbers (Table 2), but nevertheless very different distributions of gold (Fig. 6). In drill core 89-09 the main gold peak is in the Pd1/Au level, in drill core 89-09A in Pd1/Au as well as in a small peak c. 1 meter above, and in 89-09B the main gold peak is elevated c. 3 m above Pd1 (Fig. 6). Major local variations are seen in the distribution of gold relative to the Pd1 peak.

In data sets high stratigraphic resolution, the first Cu peak (Cu>1000 ppm) always occurs *above* main the Au-peak and identifies the base of the Cu-dominated uppermost part of the mineralisation (CuM, as defined in Nielsen *et al.,* 2015). The base of CuM is the

stratigraphic level at which mineralisation levels change from Au-rich to Cu-rich, irrespectively of the stratigraphic position of the Au-peak relative to the leucocratic layers of MLs. It is below leucogabbro L1. of the Triple Group at the margins and above L2 in the centre of the intrusion (Fig. 3a).

A much simpler geochemical subdivision of the mineralisation was proposed by Holwell & Keays (2014). They correlate PGE and Au anomalies across the intrusion and irrespectively of the relative stratigraphic elevation, and defined a Pd-zone with an underlying Subzone (both PGE rich) an intermediate zone with an increasing number of Pd-levels toward the centre of the mineralisation, and a capping gold zone at the transition to the overlying Cu-rich mineralisation. The proposed gold zone would be diachronous and discordant. It rises from the margin to the centre upwards through ~40 m of stratigraphy (including four MLs) of the Triple Group (Fig. 3a). It would encompass gold-rich parts of the PGE-saucers of Nielsen *et al.* (2015) as well as little-mineralised gabbros between gold-rimmed PGE-saucers in the succession of MLs (Figs 3-4).

Reported precious metal parageneses

The volumetric proportion of sulphide in the mineralisation is very small and, in samples that have precious metal concentrations in the ppm range it is estimated to be ~0.05 vol. % (Rudashevsky *et al.*, 2014, 2015; Nielsen *et al.*, 2015; Holwell *et al.*, 2016). The sulphides are almost exclusively Cu-rich and are dominated by bornite, chalcocite, digenite, and minor chalcopyrite. Pyrrhotite, cobaltpentlandite, pentlandite, sphalerite, arsenopyrite, pyrite all are very rare (Rudashevsky *et al.*, 2014 and 2015; Nielsen et al., 2015; Holwell *et al.*, 2016).

Initial information on the precious metal paragenesis is provided by Bird *et al.* (1991), Andersen *et al.* (1998), Cabri *et al.* (2005), and Nielsen *et al.* (2005) who summarized

the then available mineralogical information from 6 drill cores and reported the occurrence of >30 precious metal minerals and phases (Nielsen et al, 2003_{a-e}; Rudashevsky *et al.*, 2004). The mineralogy is very varied and comprises a large number of known minerals, frequently recorded stoichiometric compositions that are possible unnamed minerals or intermetallic compounds, and a suite of Cu and precious metal-bearing alloys. Subsequent mineralogical investigations presented by Rudashevsky *et al.* (2005_{a-b}, 2006_{a-b}, 2009a-b, $2010_{a-d,}$ $2012_{a-i,}$ 2014 and 2015), Nielsen *et al.* (2015), McDonald *et al.*, (2008) and Holwell *et al.* (2015, 2016) confirmed the complex mineralogy and add more minerals and unnamed phases to the list. All of these reports and investigations are the basis for the 3D compilations and interpretations of the parageneses of the mineralisation of this contribution.

Common minerals and phases of the Skaergaard PGE-Au mineralisation include skaergaardite (PdCu), nielsenite ($PdCu_3$), (Cu,Pd) alloys, tetra-auricupride (AuCu), (Au,Cu,Pd,Ag) alloys, (Pt,Fe,Cu,Pd) alloys electrum (Au,Ag), (Pt,Fe), seemingly stochiometric PGE and Au intermetallic compounds, a large variety of non-stoichiometric PGE and Au-rich alloys, PGE-sulphides such as vysotskite ((Pd,Ni,Cu,Fe)S), braggite ((Pt,Pd,Ni)S), and vasilite ($(Pd,Cu,Fe)_{16}S_7$), arsenides, such as guanglinite ($(Pd,Pt)_3(As,Sn)$) and arsenopalladinite ($Pd_8(As,Sb)_3$), tellurides such as keithconnite (Pd_3Te), stannides like atokite (Pd_3Sn), and the plumbide zvyagintsevite (Pd_3Pb). In the fully developed central part of the mineralisation the precious metals are hosted in skaergaardite (PdCu) and in tetra-auricupride (AuCu) and related intermetallic compounds. Pt-rich minerals are exceedingly rare.

Methods and data sources

Investigation of mineral parageneses

The precious metal mineral grains of the Skaergaard PGE-Au mineralisation are generally so small (<5 to ~100 micron, averages of 15-20 micron; Rudashevsky *et al.*, 2014, 2015) that they easily escape observation under the microscope. To overcome this difficulty, the precious metal parageneses were studied from Hydroseparator® concentrates (Cabri *et al.*, 2005) of sulphide and precious metal grains in monolayer samples (polished thin sections or mounts). A total of 32 samples were investigated (EA5), and more than 4000 grains were studied using a Camscan Microspec-4DV scanning electron microscope equipped with a Link AN-10,000 detector (Cabri et al., 2005). The samples included three bulk samples from "Toe of Forbindelsesgletscher" (locality ToF in Fig. 1a; unofficial name) investigated by Skaergaard Minerals Corporation (Cabri, 2004b), and 29 drill core samples from four separate drill cores (Rudashevsky *et al.*, 2014 and 2015, Tables 3-5). The drill cores selected for the study include 90-10 from the western margin of the intrusion, 90-18 from the SW part of the mineralisation, 90-24 from the centre of the mineralisation (sister core to 90-22 that was sampled by Bernstein & Nielsen (2004), Nielsen *et al.* (2015), and part of the sample collection used by Keays &Tegner (2016)), and 90-23A from the eastern margin (see Fig. 1a for locations).

Whereas the concentrates of precious metal grains in the bulk samples were obtained by performing the Hydroseparator® technique on a split and sieved fraction of 1-tonne samples, the samples from drill cores represent all of the precious metal grains that were retrieved from a 1-metre section of drill core. For each drill core-sample, this amounted to between 600 and 1200 g of gabbro, which varied due to lithology and previous use of the core for exploration purposes. In samples with the highest precious metal grades (>3 ppm) we commonly retrieve several hundred precious metal mineral grains from a single 1-meter sample. Information collected from the samples includes backscatter images, grain size, paragenetic information, and for each individual grain, the composition and volume, which was estimated

from the size of a circle that enclosed the grain (a method comparable to that of Holwell *et al.*, 2016). The primary mineralogical data for the present compilations are available in reports (Nielsen *et al.*, 2003_{a-e}; Rudashevsky *et al.* 2005_{a-b}, 2006_{a-b}, 2009a-b, 2010_{a-d}, 2012_{a-i}) on the "Greenland Portal", at www.greenmin.gl (official web page of Greenland Minerals Authority) Compiled tables with lists of the precious metal minerals and phases in mineralisation levels (Pd6 to Pd1/Au and Au+1) in drill cores and bulk samples across the intrusion (E-W section) and the volumetric proportion of the minerals and phases in MLs in the mineralised intervals are provided in EA5-EA12.

In this contribution we have summed up the relative volumes for: a) PGE-rich alloys, b) PGE-rich sulphides, c) PGE-rich arsenides, d) other PGE-rich minerals and phases with Sn, Bi, Pb, Te, Se, Sb, a.o., and e) Au and Ag minerals and phases throughout the mineralisation. The tables also report the depth of the Pd5 peak in the drill core from which the sample was taken, the name of the mineralisation level for a given sample (see Fig 3a), the elevation of the sample relative to nearest Pd-peak, elevation of sample relative to Pd5 peak, and the number of grains that were studied from the given sample. In addition, EA6-EA11 include descriptions of the precious metal parageneses of individual samples.

Geochemical sources

The geochemical data presented in Table 6, is compiled and refined from assays reported by Platinova A/S (Watts, Griffis & McOuat, 1991), Skaergaard Minerals Corporation (Hanghøj, 2005), Holwell & Keays (2014), and drill core 90-22 (Bernstein & Nielsen, 2004, EA13). These references for the precious metal assays include information on the analytical methods used, and details of the sampling methods for those data sets.

The geochemical profile obtained from drill core 90-22 is used for the principal component analysis (Fig. 12, Table 8, EA14), and is composed of a continuum of 25-cm samples (Bernstein & Nielsen, 2004; 259 samples, 258 analysed for Pd, Pt and Au, EA13) and serves as 'master profile' for the identification of the MLs and mineralisation levels in the central parts of the Skaergaard PGE-Au Mineralisation. Being an integrated part the standard profile for the intrusion (Tegner *et al.*, 2009), the data set in Keays & Tegner (2016), drill core 90-22 allows correlation between all these studies. It is the only publicly available, continuous data set for density (Fig. 5) and full major-, trace-, and precious metal (Pd, Pt and Au) element geochemistry through the fully developed centre of the Skaergaard PGE-Au Mineralisation.

All cores drilled in the Skaergaard intrusion have numbers that identify the year they were drill and a consecutive number (e.g. 90-22, drill core 22 drilled 1990). The numbering system was adopted by Platinova Resources Ltd in 1989 and has been continued by all other license holders. Drill cores 89-01 to 90-27 were drilled by Platinova Resources Ltd. and Platinova A/S, drill cores 04-28 to 04-34 by Skaergaard Minerals Corporation (SMC), and drill cores 08-35 to 11-58 by Platina Resources Ltd. All exploration reports and assay data in public domain are all available online in “Greenland Portal” at www.greenmin.gl.

Compiled information

The precious metal parageneses of the Skaergaard PGE-Au Mineralisation.

The mineralogical investigations listed above show that the parageneses of the Skaergaard PGE-Au Mineralisation comprise a total of 3 native elements, 35 precious metal minerals, 21 repeatedly recognized precious metal phases, and about 40 alloys combining two or more of PGE, Au, Ag, Cu, Sn, Zn, Ni, Fe Sb, Pb, Ge, Te, and S (Table 3). Pt-minerals and phases are very rare and Pt is almost entirely hosted in Pd-minerals and phases. The paragenetic variations

for individual drill cores and MLs (i.e. in the order that the host rocks accumulated) are summarise in Fig. 7 and Table 4. All volumetric percentages are reported relative to the total volume of the precious metal paragenesis of the studied sample. The distribution of investigated samples and detailed descriptions are found in EA5-EA12.

Near the margins of the intrusion, precious metals are restricted to ML0 and ML1.1. At the western margin (drill core 90-10) the precious metal assemblage is dominated by the PGE-sulphides vysotskite and vasilite, PGE-arsenide guanglinite and Au-minerals including Au-rich intermetallic compounds and/or alloys. At the eastern margin (drill core 90-23A) the paragenesis is dominated by the Pd-plumbide zvyagintsevite, Pd-arsenides guanglinite and arsenopalladinite, and unnamed Au-alloys. In both drill cores the proportion of the dominant Pd-phase (as sulphides in the west and plumbide in the east) decreases upward and is volumetrically replaced first by arsenides, and then by Au-rich phases (Table 5, Fig. 7). In ML1.1 at both the east and west margins, the parageneses are strongly dominated by Au-phases (alloys of Au, Pd, Cu, Fe and Ag) and Ag-phases. The overlying mineralisation levels in the same cores are Cu-rich and poor in precious metals (e.g, drill core 90-23A in Fig. 3a).

In more centrally located sampling sites (drill core 90-24 and bulk sample TOF) the PGE-paragenesis of the main PGE peak in ML0 (Pd6 and Pd5) is dominated by skaergaardite (PdCu, >95 vol. %), and the remainder is accounted for by related alloys. In the south-western part of the intrusion, ML0 in drill core 90-18 is characterised by a mixture of PGE sulphides (18.2 vol. %, vysotskite dominates) and Skaergaardite and related alloys (78.0 vol. %), and therefore can be considered transitional between the skaergaardite dominated centre and the sulphide dominated W-margin (Table 4 and Fig. 7).

With minor departures, the mineralogy of the precious metal mineral assemblages in overlying MLs in the central sampling sites (drill core 90-24 and TOF) continue to be

dominated by skaergaardite (PdCu). With increasing height in the stratigraphy, an increasing amount of Au is substituted into skaergaardite in place of Pd (Rudashevsky *et al.*, 2014) until skaergaardite is joined, or substituted, by tetra-auricupride (AuCu). In drill core 90-18 from the SW part of the intrusion, the relative volumes of the sulphides vysotskite and vasilite increase with stratigraphic height until the uppermost mineralisation levels (those above ML2.2, five MLs above the base of the mineralisation), where the assemblage is dominated by Au-phases. In parallel with the observations at the margins, the dominant Au-phases in the centre of the mineralisation are tetra-auricupride and (Au,Cu,Pd) intermetallic compounds, with compositions between skaergaardite (PdCu) and tetra-auricupride (AuCu). Tetra-auricupride and Au_3Cu dominate the Au-rich mineralised levels in ML2.2 in drill core 90-18, as in the uppermost Au-rich levels in drill core 08-35A (Holwell *et al.*, 2015) some 40 m lower in the succession of the layered gabbros (Fig. 7, EA12). The uppermost part of the Au-mineralisation is, irrespectively of stratigraphic elevation above the main PGE peak (Pd5) and the ML it is hosted in, characterized by unnamed Au_3Cu.

Bulk rock PGE and Au: E-W cross section

In order to provide an overview and a better understanding of the distribution of precious metals in the mineralisation we have calculated grade times width numbers (g*w) for all drill cores for which assays are publicly available. The (g*w) number for a given interval of a drill core is the average concentration in the chosen width or stratigraphic interval in grams/ton (ppm) multiplied by the width or height of the interval in metres, and is equivalent to compositing the selected stratigraphic interval of the mineralisation into a 1-meter thick layer of gabbro containing all precious metal of the stratigraphic interval. We include: (1) (g*w) for the main PGE mineralisation level (Pd5), which is defined as the 5 m of core with the highest 1-m (Pd+Pt)

averages and equivalent to the Pd-zone of Holwell & Keays (2014); (2) (g*w) for LPGEM (Fig. 5), which includes the lower Pd6-Pd4 mineralisation levels in ML0 and ML1.1 as defined by a cut off at 100 ppb (Pd+Pt) below Pd6 and the PGE-low between mineralisation levels Pd4a and Pd3b of the mineralisation (see Fig. 3a). Following Nielsen *et al.* (2015), LPGEM is the stratigraphic interval of gabbro that crystallised while precious metals were supplied to the mushy floor of the intrusion; and (3) (g*w) for the total stratigraphic interval of the precious metal mineralisation, comprising the drill core section between a lower cut-off of 100 ppb at the base of Pd6, and an upper cut-off of 100 ppb at the top of the precious metal mineralisation of a given drill core.

For the entire precious metal mineralisation (case 3 above), the (g*w) for (Pd+Pt+Au) increases from ~25 near the margins to >45 in the centre of the mineralisation (Fig. 8, Table 6). These concentrations signal results from increases in the Au and PGE (Pd+Pt) grades towards the geographic centre and up the MLs (Figs 8-10). For LPGEM (Pd6-Pd4, case 2 above), the Pd+Pt (g*w) number is 21-22 across the intrusion, with Au (g*w) decreasing from highs of ~4 at the margins (5.4 in drill core11-57; Holwell & Keays, 2014) to a low of 0.8 at the centre of the intrusion (Table 6), and complementary to what is observed for the entire stratigraphic interval of the mineralisation (Fig. 9). In Pd5 (case 1 above) the (g*w) for (Pd+Pd) decreases from a high of c. 11 at the margins (note, however, Holwell *et al.* 2016 recorded a maximum of >14 for Pd in drill core 08-35A, but supply no data for Pt) to < 9 in the geographically central parts of the mineralisation. The Au (g*w) in Pd5 decreases from approximately 0.75 at the margins to 0.35 at the centre. Thus the Pd5 interval, just as LPGEM displays a distribution that is complementary to total of precious metals contained in the mineralisation (case 3).

Apart from the most westerly drill core (90-18) all open symbols in Fig. 8 refer to (g*w) numbers from drill cores that are located north of the cross section (from W to E: drill cores 04-30, 89-03, 89-04, and 89-06; see Table 6). Their low totals are artefacts of greater distances to the geographical centre of the concentric mineralisation. Drill core 90-18 (1200m from W margin) with elevated precious metal contents is located far to the SW in the mineralisation (Fig. 1a), but projects too close to the western margin despite a more central location in the mineralisation. It should be compared to more centrally located drill cores.

Bulk rock PGE and Au relative to centre

The distribution of precious metals in the mineralisation is concentric (Fig. 4, Andersen *et al.*, 1998; Watts, Griffis & McOuat, 1991) and the elemental distribution is better illustrated relative to a possible centre for the mineralisation (Fig. 10). The location of the centre is, however, not well-constrained. Here we have, in part supported by Watts, Griffith & McOuat (1991) and by trial and error used topographic fixed point 666 on the western side of Basistoppen and between the drill hole collars of drill core 90-22 and 90-24 as a proxy (Fig. 1a, see also exploration map in Watts, Griffis & McOuat, 1991). In the compilation of the available data from 24 drill cores we include (g*w) for PGE (Pd+Pt) and total precious metals (Pd+Pt+Au) as well as the three elemental ratios Pd/Pt, Au/Pt and Au/Pd for the stratigraphic interval between cut-offs of 100 ppb (Pd+Pt+Au) at base and top of mineralised gabbros, for LPGEM, and for Pd5. From the margin of the intrusion to the geographical centre of the mineralisation the (g*w) for (Pd+Pt+Au) increases from ~25 to >45 in and is accompanied by increases in Au/Pt and Au/Pd. This pattern signals a general enrichment in Au whereas Pd/Pt shows only a very limited increase toward the centre.

The main PGE mineralisation level (Pd5) is complementary. Drill cores near the margins of the intrusion show high (g*w) for (Pd+Pt) and (Pd+Pt+Au) compared to most of the cores from the geographical centre (Fig. 10). The Au/Pd and Au/Pt ratios decrease markedly towards the centre and is combined with a general decrease in PGE (see above), which indicates a strong relative depletion in Au in Pd5 in the centre. In LPGEM the (g*w) numbers are intermediate between numbers for Pd5 and those for the entire mineralisation between 100 ppb cut offs above and below the mineralised gabbros. LPGEM shows little variation in (g*w) from margins to centre in (Pd+Pt) and (Pd+Pt+Au) and in the Pd/Pt ratio, whereas the Au/Pt and Au/Pd ratios - as in Pd5 – are in comparison high near the margins of the intrusion and reflect general Au depletion in LPGEM toward the geographical centre.

Precious metal to copper ratios in LPGEM

The ratio (Pt+Pd+Au)/Cu computed from whole rock analyses (Table 7; Fig. 11) is a proxy to the average (Pt+Pd+Au)/Cu of the sulphide droplets once hosted by the bulk rock as precious metals are heavily partitioned into the sulphide melt. Since this ratio reflects the sum of the processes that affected the composition of droplets of sulphide melt during the crystallisation of the local gabbroic host, any variation of (Pt+Pd+Au)/Cu within a specific stratigraphic interval across the intrusion will likely point to differences in the local physical and chemical processes during crystallisation. Figure 11 shows how (Pt+Pd+Au)/Cu varies across the intrusion for the interval between 8 m below the Pd5 peak to 4 m above it, corresponding roughly to the zone spanned by ML0. The data shows how (Pt+Pd+Au)/Cu increases from the margins towards the geographical centre of the mineralisation at all depths, and that (Pt+Pd+Au)/Cu at the centre is greater than that at the margins by a factor of up to 2.2. Importantly, this difference is present

despite the inwards depletion of Au (and to a lesser extent, Pd) in Pd5 and the LPGEM (Fig. 10, Table 6) and is due to a significantly lowered Cu relative to the precious metals.

Principal component analysis

To examine the mineralisation in the context of the host rock and test models for the distribution of the precious metals, we performed a principal components analysis (PCA) on assay data from drill core 90-22. The aim of a PCA is to reduce the dimensionality of a dataset by extracting from it a set of linearly uncorrelated variables, or principal components, and retaining only those that make significant contributions to the total variance. Detailed descriptions of the PCA methodology are given by Le Maitre (1982) and Albarède (1995), and some additional, recent examples of its application to igneous geochemistry are given by, e.g., Hamelin *et al.* (2011), Ueki & Iwamori (2017). The interval 978.5-1045 m from drill core 90-22 from the centre of the mineralisation (Bernstein & Nielsen, 2004) was used for the PCA because it comprises the thickest and most fully developed sequences of mineralisation for which both lithochemistry and precious metal assays exist. The dataset comprises 258 samples.

To prepare the data for the PCA, all trace elements were converted to parts per million concentrations, and major element oxides were recast as their major element cation values. Because geochemical datasets are compositional by nature and contain only relative information, the data in their raw form are subject to spurious correlations (e.g. Aitchison, 1986; Aitchison & Egozcue, 2005; Pawlowsky-Glahn & Egozcue, 2006). To avoid these well-documented effects and reveal meaningful correlations, the data were transformed using the centred log-ratio transformation (Aitchison, 1982) and subsequently scaled and centred. To improve the performance of the PCA the data were filtered to (i) remove variables that do not correlate significantly with other variables, and (ii) replace sets of variables that show very

strong multicollinearity, such as REE, with a single variable from the set. This resulted in the selection of the following 14 variables for the PCA: Ti, Fe^{3+}, P, Pd, Pt, Au, V, Cu, Zn, Y, Zr, Ce, Nd, and Pb (see EA13). Finally, these variables were extracted from the original data set and the centred log-ratio transformation was reapplied.

Table 8 summarizes the results of the first 6 principal components of the PCA (full results in EA14, Table EA14-1). Application of the scree test (Cattell, 1966) indicates that the first 3 principal components (PCs) provide a meaningful representation of the input data; collectively they explain 80% of the total variance of the data. To aid analysis and interpretation, Figures 12a-c plot for each of the three PCs the standardized loadings of the different elements considered, and figure EA14-3 in EA14 shows how PCs 1-3 vary with depth in drill core 90-22. In Figures 12a-c and EA14-3 and Table 8, the loadings indicate how each element correlates with the different principal components. For example, large positive values indicate that a given analyte and principal component correlate positively and strongly. Conversely a small magnitude, negative value indicates a weak, negative correlation between a component and analyte.

PC1 accounts for 45% of the total variance. From Figure 12a and Table 1 it is clear that this component discriminates between aspects of the precious metal mineralisation and, with the exception of Cu, elements that are typically found in silicate, oxide and phosphate minerals. That copper and the precious metals Pd, Pt and Au are anticorrelated in this component indicates that more processes are responsible in determining the distributions of these metals within the mineralized section of Skaergaard. Figure EA14-3 demonstrates that local lows in PC1 correspond to mineralisation levels Pd2-6, Pd1 and to lesser extend Pd1/Au.

In PC2, which accounts for 26% of the total variance, Fe3+ and the metals Ti, V, Zn correlate strongly and negatively with Au, and the relatively incompatible elements P, Pb, Ce

and Nd (Fig. 12b). Cu does not participate in PC2, and the remaining precious metals (Pd and Pt) and Zr are only weakly associated with the component. Systematic variation in PC2 with depth (Fig. EA14-3) is less obvious than for PC1. PC2 increases to the top of ML0 and ML1.1, in Pd3a and b peaks of ML1.2, but has minor importance in ML2. The largest and distinct positive values of PC2 occur in ML2.1 in the top 15 m of the studied interval and form local highs at the stratigraphic positions of Pd1 and especially at Pd/Au.

PC3 accounts for 9% of the total variance of the data. Figure 12c shows that Au and Cu correlate strongly and positively with PC3. Fe3+ and Pb also load positively, but more weakly, onto this component. These metals (including Fe3+) are anticorrelated with P, which exhibits the largest negative loading in PC3, and, to a slightly lesser extent, Pd, Pt and Ce. The remaining metals (Nd, Ti, V, Y, Zn, Zr) load very weakly and negatively with PC3. Figure EA14-3 shows that the variation of PC3 with depth is complex. The variation is in general more systematic above ML1.2, corresponding to the interval spanned by UPGM, UAuM and CuM <1021m). In ML1.2 and ML2 the PC3 loadings generally decrease with height above a Pd interval before increasing within a few metres of the next overlying Pd level. The largest positive values occur again in the top 15 m of the studied interval and correlates with elevations in Cu concentration >200 ppm).

Discussion

Sulphide saturation as the driver for mineralisation

To understand the results it is necessary to review the evidence for sulphide saturation as the driver for the mineralisation process. Models proposed for origin of the Skaergaard PGE-Au Mineralisation include: (1) contamination/mixing-driven sulphide saturation and precious metal deposition (Bird *et al.*, 1991), (2) mineralisation caused by upward transport and re-deposition of

precious metals by rising (silicate melts and/or fluids late in the solidification of the gabbros (e.g., Boudreau, 2004) , and (3) closed magma chamber fractionation of melt to sulphide saturation (Andersen *et al.*, 1998; Andersen 2006; Nielsen *et al.*, 2005, 2015; Holwell & Keays, 2014; Holwell *et al.*, 2015, 2016; Keays & Tegner, 2016). Together, these models cover almost the entire spectrum of processes suggested responsible for PGE mineralisations in layered mafic intrusions.

In the Skaergaard intrusion, the section of MZ beneath the mineralisation includes several stratigraphic intervals that are distinguished by both (i) elevated, but erratic Pd concentrations (Andersen *et al.*, 1998; Nielsen *et al.*, 2015), and (ii) the presence of many gabbroic blocks, which originate from a collapsed part of the UBS and are estimated to make up about 10 vol. % of lower MZ (Irvine *et al.*, 1998). The variation in (Pd+Pt) and in Pd/Pt in the block zone is seemingly of local origin as it returns to low values in bulk rocks above the block zone (Nielsen *et al.*, 2015) and the elevated precious metal grades are suggested to be caused by local contamination- or mixing-driven accumulation of precious metal-bearing droplets of sulphide melt. This was first suggested by Bird *et al.* (1991), who proposed that incorporation of the gabbroic UBS blocks led to an increase in crystallisation of FeTi-oxides and to decrease FeO* and in sulphide solubility in the silicate melt. However, the main PGE-Au mineralisation contains fewer as well as large roof blocks (Fig. 2) but shows concordant variations across the intrusion (EA1), irrespective of the frequency of UBS blocks and lateral variations in grades and elemental ratios of precious metal (Fig. 10). The Skaergaard PGE-Au mineralisation demonstrates no clear evidence is for a magma mixing- or contamination-driven sulphide saturation

Other models suggest that precious metals were scavenged from already-crystallized gabbros by upward migrating late-stage fluids, and then redeposited, e.g. at redox

barriers, (Boudreau, 2004; Boudreau & Meurer, 1999). These models are also regarded unlikely because sulphide droplets with PGE and Au are found inside liquidus phases of the gabbroic host (Godel *et al.*, 2014; Nielsen *et al.*; 2015, Holwell *et al.*, 2016). Only the late deposition of Au on grain boundaries in extensively crystallised gabbro (UAuM) could be caused by a late, residual and upward migrating, volatile-rich silicate melt and fluids (Godel *et al.*, 2014; Nielsen *et al.*, 2015; Rudashevsky *et al.*, 2014).

This leaves the possibility for sulphide saturation caused by closed system fractionation. This is supported by the mineralogical investigations and the PCA model. The major difference between the proposed sulphide saturation models is that Holwell *et al*. (2016) assume sulphide saturation in bulk liquid, whereas Nielsen *et al.* (2015) restrict sulphide saturation to evolved mush melts of the crystallisation zones that existed between remaining bulk liquid and already crystallised gabbros. The timing of sulphide saturation in the evolution of the bulk liquid therefore is a key question that needs to be addressed. Keays & Tegner (2016) suggested that sulphide saturation in the bulk liquid was reached at the evolutionary point represented by the liquidus paragenesis represented by LZc (t_{LZc}). As noted in Nielsen *et al.* (2015), however, co-variations in Pd/Pt and Au/Pt in the bulk liquid prior to the mineralisation in upper MZ point to loss of Pt rather than Pd or Au, during crystallisation of LZc and up MZ, e.g. in the form of ferroplatinum ((Fe,Pt); Holwell *et al*., 2016). If sulphide saturation had taken place from t_{LZc} and onwards, the Pd/Au ratio should have decreased in the remaining bulk liquid throughout LZc and MZ because $D_{Pd} >> D_{Au}$ for coexisting sulphide and silicate liquids. With the exception of minor deposition of PGE in MZ in reaction with sunken roof blocks, a decrease in Pd/Au is not observed (Nielsen *et al.*, 2015), and thus the initiation of sulphide saturation in bulk liquid at t_{LZc} is not supported.

Only the closed system sulphide saturation models in Nielsen *et al.* (2015) and Holwell *et al.* (2016) seem plausible, but they are based on very different perceptions and samples sets. The Nielsen *et al.* (2015) model is based on drill cores from across the intrusion, and is inherently three dimensional as a result and times mineralisation processes relative to the crystallisation of the silicate host rock. The study and conclusions of Holwell *et al.* (2016) are based mainly data obtained from drill core 08-35A from near the margin of the intrusion and seemingly assumed to be representative for the mineralisation process throughout the intrusion. The stratigraphic variations in Fe_2O_3 in sections of drill core (Fig. 13) are proxies to the lithological variation in the layered host rocks of the mineralisation and allow detailed correlation between the sections of drill core studied by Holwell *et al.* (2016) and Nielsen *et al.* (2015). The entire stratigraphic interval enriched in precious metals (from the Subzone to Au-zone of Holwell *et al.*, 2016) in drill core 08-35A from near the margin of the intrusion corresponds only to a 20 m succession of gabbro in ML0 and ML1.1, and to LPGEM with mneralisation levels Pd6, Pd5, Pd4a and Pd4b of central drill core 90-22 (Fig. 13).

In contrast the precious metal mineralisation in the centre of the intrusion is in all drill cores (except drill core 90-18, which hosts an additional upper Au-rich level) contained within a stratigraphic interval 60 m thick. It includes five MLs (rather than two) with precious metal peaks in Pd-levels Pd6 to Pd1 and Pd1/Au (Figs 5). The package of MLs maintains near constant stratigraphic thickness across the floor of the intrusion (EA3) and the profile through the mineralisation discussed in Holwell *et al.* (2016), therefore, is not a compressed version of the section studied by Nielsen *et al.* (2015).

Evidence against offset reef-style mineralisation

Near the margin of the intrusion, in drill core 08-35A, the uppermost PGE peak is in Pd-level Pd4b (~5 m above the main Pd peak in Pd5, see fig. 5 in Holwell et al, 2016) and the Au peak ~7 m above Pd5. However, in the Middag Buttress chip line (Fig. 3a) and as well as the incompletely sampled Midnat chip line (Turner & Mosher, 1989; Fig. 2b) to the north and farthest away from the centre of the deposit (see locations in map Fig. 1a), PGE and Au are accumulated in the same one-metre interval of layered gabbro that hosts Pd5 throughout the intrusion.

The marked differences between the margin and the centre of the mineralisation is also shown by (g*w) for the uppermost Au rich part of the mineralisation (Table 6; Fig. 12). In the centre the combined Au-bearing Pd1, Pd1/Au and UAuM mineralisation levels have 2.1 g/t precious metals over 3.6 m at a cut off of 0.7 g/t and a (g*w) of 7.56 whereas the drill core from the margin of the intrusion that Holwell *et al.* (2016) presents as representative for the Skaergaard PGE-Au Mineralisation has an average of 2.2 g/t over 0.8 m and a (g*w) of 1.76. That is less than 25% of contained gold compared to the centre of the deposit. The drill core studied in Holwell *et al*. (2016) does not compare to and cannot be representative for anything but the Skaergaard PGE-Au Mineralisation as developed at the east margin of the intrusion.

As mentioned above, the accumulation of precious metals during the formation of offset reef type mineralisations is thought to be concordant with the crystallisation front. Holwell *et al.* (2016) and Holwell & Keays (2014) attribute the formation of their Au-zone to a single, short-lived and critical event, but this scenario is difficult to reconcile with the increase in stratigraphic elevation between the peak PGE and peak Au concentrations, from <1 m farthest away to >43 m at the centre of the mineralisation, whilst the host layered gabbros form a concordant succession of MLs that maintains constant stratigraphic thickness across the intrusion (Fig. 3a and b, EA3). Assuming a constant crystal accumulation rate of 2 cm/y on the

floor of the intrusion (Irvine, 1970; Morse, 2011) the Au and PGE (Pd5) peak are separated by >2000 years (y) in the centre of the intrusion (e.g. drill core 90-22, stratigraphic separation of 40 m, see SD3 of Nielsen *et al.*, 2015), 400 y closer to the margin (e.g. drill core 08-35A, stratigraphic separation of 8 m, Holwell *et al.* 2016) and <50 y farthest away from the centre of the mineralisation (e.g. Middag and Midnat Buttress chip lines, stratigraphic separation <1 m). Assuming the crystallisation rate in upper MZ had dropped to 1 cm/y during the later stages of crystallisation when only 20% of the initial volume of bulk melt remained, the precious metal mineralisation may have formed over as much as 4000 years; thus its formation would have been diachronous. In the context of an offset reef-type model, this situation is not compatible with a mineralisation event triggered by a specific and short-lived event in a magma homogenized in convective currents (cf. Holwell *et al.*, 2016).

Accumulation of precious metals in the floor mush.

As an alternative to the classic offset reef type models, Nielsen *et al.* (2015) suggested that the structure of the mineralisation, and temporal and elemental correlations were the result of syn-magmatic accumulation and re-distribution of precious metals in an upward migrating and stratified mush zone in the floor of the magma chamber (Nielsen *et al.*, 2015). The diachronic distribution of PGE and Au (Figs 3a, EA1, EA4) is by these authors regarded critical and taken to demonstrate redistribution of precious metals up the succession of MLs. They also argued that initial accumulation of precious metals in the floor mush was due to scavenging of precious metals by immiscible droplets of sulphide melt (small and in suspension) in the crystallising and evolving bulk melt that convection carried along the mushy roof of the magma chamber. At immiscibility between Fe-rich and Si-rich silicate melts in this mush and after the buoyancy-driven loss of the Si-rich conjugate, the sulphide solubility increased in the remaining

Fe-rich silicate melt. In consequence, already formed droplets of sulphide melt dissolved in the Fe-rich conjugate. The dense Fe-rich melt mixed with crystals and was carried to the floor of the magma chamber by convection. The precious metals were subsequently redistributed into MLs during the upward migration of the mushy crystallisation zone in the floor of the magma chamber. Precious metals were supplied to the floor during the crystallisation of ML0 and ML1.1 (LPGEM) only, as MLs above ML1.1 (UPGEM) near the margins of the intrusion are Cu-rich and only have traces of precious metals (Fig. 3a, Nielsen *et al.*, 2015).

A simple upward re-deposition of precious metals that were initially evenly distributed across the floor of the magma chamber cannot account for the total of precious metals accumulated in the central parts of the mineralisation (Fig. 8, Table 6). The (g*w) of the precious metal reaches a maximum of ~50 with ~38 for PGE and ~12 for Au in the centre, compared to 18-20 for PGE and 4 for Au closer to the margins (Fig. 10, Table 6). These results show that distribution of precious metals in the mineralisation requires pre-concentration of precious metals in the central part of the bowl in the floor of the magma chamber.

Ponding of precious metal bearing silicate melt (e.g. Holwell & Keays, 2014) could potentially account for the increasing larger (g*w) numbers and a stratigraphic separation of >40 m between PGE and Au rich mineralisation levels (Fig. 3a) in the centre of the mineralisation. A bowl constructed from observed Au peaks, however, would in its centre be >600 m deep relative to the rim and the ponded magma should therefore itself have the shape of a >600 m deep bowl. However, the distribution of ponded melts is controlled by gravity and would not form a >600 m deep bowl with walls thinning from forty to a few metres from the centre of the bowl and >600 m up the walls of the magma chamber. An alternative suggestion could be a bowl formed by accumulation of precious metals over thousands of years with increase in Au, and accumulation gradually displaced to more central parts of the magma

chamber. Such a scenario would, however, be in conflict with overlapping PGE and Au peaks farthest away from the centre of the mineralisation and would not explain why gabbro successions that formed at the same time (same ML layer and same Pd-level, e.g., Pd2b in Fig. 3a) contains PGEs in the centre, Cu-sulphides at the margin of the intrusion and Au in between (Fig. 3a).

The explanation we suggest for the increase observed in (g*w) numbers in the central parts of the mineralisation is that slurries composed of Fe-rich silicate melt and solids descended along the walls of the magma chamber and decelerated as they reached the bowl-shaped floor. During deceleration the slurries deposited carried-along solids (crystals) while Fe-rich and dense silicate melt with its load of dissolved precious metals continued into the deeper part of the bowl-shaped floor. In itself, the bowl-shape is witness to a continued accumulation of solids entrained in convection currents descending along the concomitant walls of the magma chamber. The preservation of near-constant thicknesses of MLs in Triple Group despite the accumulation of entrained solids near the walls may seem as a contradiction, but is apparently the consequence of the dynamic stratification process in the MLs of the Triple Group (see section: Macro-rhythmic layers and compositional subdivision). At the time of formation of the mineralisation, the density of the mush melt was less than that of pyroxene and FeTi-oxides, but greater than that of plagioclase (see fig. 26 in Nielsen *et al.*, 2015) and *in situ* sorting of solids and melt(s) stratified the mush into a succession proto-MLs in the upward migrating mush zone. The stratification process is referred to by Nielsen & Bernstein (2009) and Nielsen *et al.* (2015) as self-stratification with thicknesses and cyclicity controlled by density contrasts and rheology (e.g., McKenzie, 2011, Bons *et al.*, 2015). The density-controlled sorting does not distinguish between crystals transported from the roof zone to the floor or those that crystallised *in situ*. The crystals would be subjected to the same dynamic forces irrespectively of their place of origin in

the magma chamber and the MLs would consequently have near-constant thicknesses across the floor of the magma chamber.

Re-distribution of precious metals in upward migrating mush melt

Paragenetic evidence for redistribution

Concentrates of precious metal grains from drill cores near the margins of the intrusion (Table 4, Fig. 7) have parageneses that are characterized by sulphides, arsenides, plumbides, tellurides, etc., and a host rock with hydrous silicate phases. In comparison, PGE parageneses in central drill cores are dominated by skaergaardite (PdCu), and gabbros that contain no hydrous silicate phases (Fig. 7, Table 4, Fig. 15a). The more varied parageneses at the margins were by Nielsen *et al.* (2015) suggested to reflect the trapping in the mushy floor of melt carrying volatiles in addition to precious metals, Cu, and elements such as Pb, S, As, and Te. Trapping of residual melt and volatiles in the gabbros near the margins was suggested to lead to re-equilibration of precious metal phases to low temperature phases such as Au_3Cu (see, Holwell *et al.*, 2016).

Equilibration of the precious metal phases with residual and hydrous mush melt, however, does not explain why gabbros close to the western contact against Precambrian basement (Fig. 1) are characterized by Pd-sulphides (vysotskite and vasilite) and arsenide-rich parageneses, whereas the gabbros at the eastern contact against Palaeogene basalts (Fig. 1) are characterized by the plumbide zvyagintsevite (Pd_3Pb) and arsenide rich Pd-parageneses (Table 4, Fig. 7), and why the same mineralisation level in the centre is entirely dominated by skaergaardite (PdCu). Skaergaardite is found as euhedral crystals within immiscible droplets of Cu-rich sulphide melt that are trapped in liquidus crystals of FeTi-oxides (Godel *et al.*, 2014; Nielsen *et al.*, 2015). These Cu-rich sulphide droplets were already depleted in most other element with distribution coefficient between sulphide and silicate liquid lower than those of

PGE, but were enriched in precious metals due to relative loss of the Cu-rich sulphide (Fig. 11). The process predated or was contemporaneous with the crystallisation of its host mineral. A further example of paragenetic variation across the intrusion is provided by drill cores 90-18 and 90-24. In drill core 90-18, Pd-sulphides are the major PGE-bearing phases, whilst in drill core 90-24, located only 2.2 km away, the paragenesis is dominated by skaergaardite and related (Pd,Cu) alloys with only traces of precious metal sulphide. The two drill cores exhibit parallel variations in bulk rock PGE concentrations (Fig. 3a), and yet they represent very different compositional environments. The precious metal parageneses are specific to a given drill core or sector of the intrusion and are found (i) inside sulphide droplets, (ii) as grains protected in and between minerals crystallised from the mush melt (Godel *et al.*, 2014; Rudashevsky *et al.*, 2014, 2015; Nielsen *et al.*, 2015), and (iii) as un-protected grains in related to subliquidus paragenesis of the gabbros (Nielsen *et al.,* 2003$_{a-e}$; Rudashevsky *et al.*, 2005$_{a-b}$, 2006$_{a-b}$, 2009a-b, 2010$_{a-d,}$ 2012$_{a-i}$, 2014, 2015). The observed precious metal paragenesis of a given sample therefore reflects the local composition of melt in in the mushy floor and the melt in which the immiscible sulphide droplets formed and equilibrated.

The observed paragenetic variations could not result from flow of melt or mushes across the floor of the solidifying magma chamber and cannot be explained by accumulation controlled by bulk liquid processes. Both would lead to more uniform parageneses in the same mineralisation levels and MLs. Instead, the paragenetic variations, just as the 3D distribution of precious metals in the mineralisation (Figs 8-10) and upward decrease in Pd/Pt in mineralisation levels (see figure 13 in Nielsen *et al.*, 2015), support crystallisation and equilibration in local geochemical environments that are repeated up the succession of MLs. The paragenetic variations in the precious metal mineralogy indicate that syn-magmatic processes in the silicate mush of the crystallisation zone vary laterally across the floor of the magma chamber in

response to local compositional variations, and that individual MLs operated as semi-closed crystallisation and fractionation chambers with limited lateral communication.

Compositional evidence for upward redistribution

In the melt-rich zones of the MLs in the floor of the magma chamber, the crystallisation is argued by Nielsen *et al.* (2015) to have driven the mush melt to sulphide saturation (leading to the formation of tiny, suspended immiscible droplets of sulphide melt and subsequently to the two-liquid field between Fe-rich and Si-rich silicate liquids. Reactions between the pre-existing silicate paragenesis and immiscible Fe-rich melt and (Holness *et al.*, 2011) would not have taken place unless the low-density granophyric conjugate was lost from the mush. The resorption of the silicate host may be comparable to dissolution processes more recently proposed in relationship to discordant chromite seams in the Bushveld Complex (Latypov *et al.*, 2017). The loss of the granophyric conjugate also led to reaction between the remaining Fe-rich melt and un-protected droplets of sulphide melt. During dissolution Pd was preferentially retained in the droplets of Cu-sulphide melt over the other precious metals, since Pd has the largest sulphide/silicate melt partition coefficient (Makovicky, 2002; Naldrett, 2011). Conversely, precious metals with lower *D*-values (Pt and especially Au) became available for convection- and crystallisation-driven redistribution upwards to the overlying MLs (Nielsen *et al.*, 2015, see also Holness *et al.*, 2017a; Vukmanovic *et al.*, 2018).

The fractionation of precious metals that is argued to have occurred during dissolution of droplets of sulphide melt is a critical step in the proposed model and is supported by the relative depletion of Au in the lower and central parts of the mineralisation (Figs 8-10) and in particular in ((Pd+Pt+Au)/Cu)*1000) in Pd5 (Fig. 11). In drill core 08-35A the ratio reaches a maximum of ~16 in the Pd5 peak (argued by Holwell *et al.*, 2016 to be the highest

among sulphide mineralisations), but in the interior of the mineralisation, up to 30 (Fig. 11). Nielsen *et al.* (2015) used petrographic observations outlined in Holness *et al.* (2011) to explain the reason for this variation. Specifically, near the margins of the intrusion, Middle Zone gabbros contain paired pockets of solidified Fe-rich and Si-rich liquids (incomplete separation of immiscible melts), whereas gabbros from equivalent stratigraphic levels near the centre of the intrusion contain abundant reactive symplectites, which are a by-product of reaction between immiscible Fe-rich silicate liquid and already crystallised gabbro. These observations indicate that the separation of the conjugate silicate melts was completed in the centre of the intrusion and allowed for reaction and dissolution of unprotected, precious metal-enriched sulphide droplets and the corresponding rise in (Pd+Pt+Au)/Cu) x 1000) in bulk rock compositions in the centre of the mineralisation.

The marked increase in precious metals during dissolution and loss of Cu is highlighted by the PCA. PC1 shows the separation of PGE (Pd and Pt) and Au from all other elements and Cu in all mineralisation levels from Pd6 to Pd1/Au (EA14). As argued by Nielsen *et al.* (2015), the mineralisation levels are melt-rich intervals in stratified crystal mush in which sulphide saturation was followed by dissolution of first-formed droplets of sulphide melt. All intervals between mineralisation levels are anti-correlated to PC1 and consequently they have no accumulation of droplets of sulphide melt formed due to sulphide saturation.

Finally, in the central parts of the intrusion, the UPGEM (Pd3b, Pd3a, Pd2b, Pd2a, Pd1, Pd1/Au and UAuM in ML1.2, Ml2, Ml2.1 and ML2.2) accounts for ~40% of the PGE over the full depth of the mineralisation (Pd6-UAuM) and for ~90% of that for Au (Table 6). This suggests that the loss of PGE and Au from LPGEM in the lower parts of the mineralisation, and redistribution of these metals to the interval spanned by UPGEM (Figs 8-10).

In combination, the (i) short-lived co-accumulation of PGE and Au in LPGEM (in Middag and Midnat Buttresses), (ii) augmented dissolution of sulphide in the central parts of the intrusion (Fig. 11), and (iii) depletion in PGE, Au and Cu in central and lowermost parts of the mineralisation (figs 8-10) demonstrate upward transport and fractionation of precious metals in a the mushy crystallisation zone in the bowl-shape floor of the magma chamber.

Late mineralisation along grain boundaries.

In the central parts of the mineralisation, the upwards increase of Au in immiscible sulphide melt is indicated by increasing Au-substitution into skaergaardite (PdCu) (Rudashevsky *et al.*, 2014) and increasing proportions of tetra-auricupride (AuCu) in the uppermost Pd-level of any given drill core (Tables 3 and 4, Holwell & Keays, 2014; Nielsen *et al.*, 2015). The clear negative value of PC1 at Pd1 (EA14) suggests sulphide saturation in mineralisation level Pd1 followed by dissolution and enrichment of remaining sulphide droplets in gold.

In addition to sulphide saturation related Au-accumulation in tetra auricupride in Pd1 and to lesser extend in Pd1/Au, all central drill cores have gold added to the uppermost Au-rich mineralisation levels. Gold is added along grain boundaries in a mineralisation event referred to as UAuM (Nielsen *et al.*, 2015). On the basis of petrography and peak concentrations at unconstrained elevations above Pd1 (see Fig. 6) UAuM is argued (Godel *et al.*, 2014; Nielsen *et al.*, 2015) to be the result of mineralisation processes caused by migration of residual silicate melts and fluids in already crystallised gabbro. We interpret the variance explained by PC2 as the result of this process. PC2 of the PCA (Table 8, Fig. EA14-3) is closely related to the Pd1 and especially to Pd1/Au peaks and above in the gold-rich top of the mineralisation in drill core 90-22 and tops ML0 and ML1.1. PC2 is anti-correlated to Cu, but correlated to P, Pb, Ce which all are incompatible elements, at least until apatite starts to crystallised from bulk liquid or mush

melts. The marked compositional differences between the gold rich Pd1 and Pd1/Au levels and all other precious metal rich mineralisation levels is highlighted in Fig. 14 that shows elevate P_2O_5 in most samples from Pd1 and Pd1/Au. PC2 is therefore on the basis of: (i) stratigraphic association; (ii) the occurrence of gold unattached to sulphide along grain boundaries, and (iii) the common occurrence of low temperature Au_3Cu (Holwell *et al.*, 2016) rather than high temperature tetra-auricupride (AuCu; Bird *et al.*, 1991) representing the separate mineralisation event referred to as (UAuM). Contrary to the conclusions of Holwell *et al.* (2016), the anti-correlation between Au and Cu in PC2 negates that all gold in the top of the Skaergaard PGE-Au mineralisation was accumulated due to sulphide saturation and accumulation of immiscible droplets of Cu-rich sulphide melt, and negates that the Skaergaard PGE-Au Mineralisation is a conventional "offset reef" type mineralisation.

The association of PC2 to incompatible elements and the enrichment in the tops of ML0 and ML1.1 (EA14) strongly support that the UAuM-type redistribution of gold was related to reactions and deposition from the residual of the Fe-rich melt ponded and crystallised within the MLs. Examination of the Au-rich mineralisation levels in exposures at Toe of Forbindelsesgletscher (ToF, Fig. 1a) and in drill core 90-22 reveals that the Au-bearing gabbros are rusty due to oxidation of Fe. The gabbroic host is in all other Pd-levels extremely fresh and shows no signs of alteration under the microscope (Fig. 15a), whereas gabbros rich in gold are affected by hydration, and extensive alteration and recrystallisation of clinopyroxene and presence of H_2O-bearing silicates (Fig. 15b).

The compositional fingerprint of UAuM is reminiscent of IOCG deposits *sensu strictu* as defined by Groves *et al.* (2010). We add that a volatile-bearing environment is evidenced by the common occurrence of hydrous phases in immiscible sulphide droplets as well as silicate melt inclusions (Godel *et al.*, 2014; Holwell *et al.*, 2016; Nielsen *et al.*, 2015). The

bulk melt of the Skaergaard intrusion was already evolved at the time of emplacement (Mg# = 0.43; Nielsen *et al.*, 2009), and only ~10 vol. % of the bulk liquid remained when immiscibility between Fe-rich and Si-rich melts was reached (Nielsen *et al.*, 2015). At the time the mineralisation formed, volatiles would have been concentrated in melt of the mushy crystallisation zones and likely amounted to several wt % (dependent on loss). It would be most surprising if the residual bulk magma was not saturated in volatiles and that no syn- to late-crystallisation redistributions in presence of a free volatile phase followed the inward migrating crystallisation zone.

Sulphide saturated mush melt in CuM

In PC3, the positive correlation between Au, Fe, Cu and Pb and anticorrelation between these elements and P and incompatibles, suggests a return to sulphide saturation. Large magnitude PC3 values occur predominantly in CuM (Fig. EA14-3). Samples from CuM are characterized by Cu-rich sulphides interstitially between grains of the host rocks and described as an orthomagmatic mineralisation (Holwell *et al.*, 2016; EA12). They apparently formed due to sulphide saturation just as Pd-levels, but without subsequent dissolution. The lack of dissolution accounts for the geochemical distinction between PC1 and PC3, seemingly because the immiscible Fe-rich melts that at CuM time ponded in the mushy floor already were sulphide saturated as they formed (cf. Nielsen *et al.*, 2015).

Sulphide saturation and subsequent dissolution (PC1) is restricted to mineralisation levels and PC3 seem to be of no importance in intervals between mineralisation levels in LPGEM and UPGEM (Fig. EA14-3). Consequently, no support is found in the PCA for sulphide saturation and accumulation of immiscible droplets sulphide melt from the bulk liquid of the Skaergaard intrusion during the formation of its PGE-Au mineralisation. Sulphide saturation was

as concluded in Nielsen *et al.* (2015) restricted to evolved melt in the mushy crystallisation zones of the magma chamber.

Conclusions

The genesis of the Skaergaard PGE-Au Mineralisation is very complex and results from *in situ* fractionation, sulphide saturation, immiscibility between Fe-rich and Si-rich silicate melts in mushy crystallisation zones in the magma chamber. The model, first developed in Nielsen *et al.* (2015) on the basis of a structural model that compares the mineralisation to a stack of gold-rimmed saucers with upward decreasing diameter, is here further supported by: i) 3D paragenetic variations of precious metal minerals, ii) 3D distribution of precious metals in the mineralisation, and iii) PC1-PC3 of the principal component analysis.

The precious metals concentrated in droplets of sulphide melt in bulk melt circulated to the mushy roof. They dissolved and were entrained in immiscible Fe-rich mush melt that descended to the floor of the magma chamber. Flow differentiation in mushes along the bowl-shaped floor concentrated melt with its cargo of dissolved precious metals in the deepest and central parts of the bowl shaped floor. The co-accumulation of PGE and Au in more distant parts of the mineralisation, the diachronous distribution of precious metals, and the lateral variations in bulk composition and precious metal parageneses in the >600 m deep bowl exclude in our view a classic offset-reef type model for the origin of the mineralisation.

In our model, the precious metals were re-distributed up the MLs of the Triple Group due to repetition in stratified mush of: i) fractionation of mush melt; ii) density stratification; iii) sulphide saturation in remaining mush melt; iv) immiscibility between Fe-rich and Si-rich silicate liquids; iv) loss of Si-rich conjugate; vi) reaction and equilibration between formed droplets of sulphide melt and ponded Fe-rich melt; vii) fractionation of Fe-rich melt and

loss of its residual taking dissolved PGE, P, REE, HFSE, Cu, Au and volatiles along to the mush of the overlying ML.

The fully developed Skaergaard PGE-Au mineralisation is neither a classic reef nor an offset reef type precious metal deposit, but a three-dimensional distribution of precious metals and the result of prolonged crystallisation, syn-depositional and syn-magmatic processes in a crystal mush. We therefore argue that the mineralisation should not be referred to as the "Platinova Reef", but to the "Skaergaard PGE-Au Mineralisation" (Nielsen *et al.*, 2015) to avoid little-supported associations to reef-type mineralisations to which its structure and genesis cannot and should not be compared. The Skaergaard PGE-Au Mineralisation is a mineralisation type in its own right.

Acknowledgements

The investigations are supported entirely by the Geological Survey of Denmark and Greenland over a period of more than 10 years. The investigations would not have been possible without the dedicated support by Leif Thorning, former head of Department at the Geological Survey of Denmark and Greenland. Most helpful reviews by Jim Mungall, Roger Scoon, David Holwell and Allan Wilson of earlier version of the manuscript are much appreciated. Susanne Rømer is thanked for preparation of illustrations.

References

Aitchison, J. (1982). The statistical analysis of compositional data (with discussion). *Journal of the Royal Statistical Society, Series B* (Statistical Methodology) **44**, 139-177.

Aitchison, J. (1986). The statistical analysis of compositional data. *Monographs on Statistics and Applied Probablity*. Chapman & Hall Ltd. 416 pp.

Aitchison, J. & Egozcue, J.J. (2005). Compositional Data Analysis: Where are we and where should we be heading? *Mathematical Geology* **37**, 829-850.

Albarède F. (1995) Introduction to Geochemical Modeling. Cambridge University Press, Cambridge, England, 543 pp.

Andersen, J.C.O. (2006). Postmagmatic sulfur loss in the Skaergaard Intrusion: Implications for the formation of the Platinova Reef. *Lithos* **92**, 198-221.

Andersen, J.C.Ø., Rasmussen, H., Nielsen, T.F.D. & Rønsbo, J.C. (1998). The Triple Group and the Platinova gold and palladium reefs in the Skaergaard Intrusion: stratigraphic and petrographic relations. *Economic Geology* **93**, 488-509.

Barnes; S.J., Holwell, D.A. & Le Vaillant, M. (2017). Magmatic Sulfide Ore Deposits. *Elements* **13**(2), 89-95

Bernstein, S. & Nielsen, T.F.D. (2004). Chemical stratigraphy in the Skaergaard intrusion. *GEUS report* **2004/123**, 31 pp. + CD.

Bird, D.K., Brooks, C.K.., Gannicott, R.A., & Turner, P.A., (1991), A gold-bearing horizon in the Skaergaard Intrusion, East Greenland. *Economic Geology* **86**, 1083-1092.

Bons, P.D., Baur, A, Elburg, M.A., Lindhuber, M.J., Marks, M.A.W., Soesoo, A., van Milligen, B. P. & Walte, N.P. (2015). Layered intrusions and traffic jams. *Geology* **43**, 71-74.

Boudreau, A. (2004). PALLADIUM – A program to model the chromatographic separation of the platinum-group elements, base metals and sulfur in a solidifying igneous crystal pile. *Canadian Mineralogist* **42**, 393-403.

Boudreau, A. E. & Meurer, W. P. (1999). Chromatographic separation of the platinum-group elements, gold, base metals and sulfur during degassing of a compacting and solidifyingcrystal pile. *Contributions to Mineralogy and Petrology* **134**, 174–185.

Cabri, L.J. (2004a). New developments in process mineralogy of platinum-bearing ores. Proceedings of the Canadian Mineral Processors, 36th annual meeting, 189-198.

Cabri, L. (2004b). A mineralogical evaluation of two samples for Skaergaard Minerals Corp, License No. 2000/10. In: Skaergaard Minerals Corporation (2004): Report on exploration activities on Skaergaard Mineral license during 2003, EA 4, 65pp. (in archive of the Geological Survey of Denmark and Greenland, GRF no. 21840; available on-line).

Cabri, L.J., Beattie, M., Rudashevsky, N.S., Rudashevsky, V.N. (2005). Process mineralogy of Au, Pd and Pt ores from the Skaergaard intrusion, Greenland, using new technology. *Minerals Engineering* **18**, 887–897).

Cattell, R.B. (1966). The scree test for the number of factors. *Multivariate Behavioural Research* **1**, 245-276.

Godel, B., Rudashevsky, N.S., Nielsen, T.F.D., Barnes, S.J., & Rudashevsky, V.N. (2014). Constraints on the origin of the Skaergaard intrusion Cu-Pd mineralisation: insights from high-resolution X-ray computed tomography. *Lithos* **190-191**, 27-36.

Groves, D.I.; Bierlein, F.P; Meinert, L.D. & Hitzman, M.W. (2010). Iron oxide copper-gold (IOCG) deposits through Earth History: Implications for origin, lithospheric setting, and distinction from other epigenetic iron oxide deposits. *Ecomnomic Geology* **105**(3), 641-654

Hamelin, C. and Dosso, L. and Hanan, B.B. and Moreira, M. & Kositsky, A.P. and Thomas, M.Y. (2011). Geochemical portray of the Pacific Ridge: New isotopic data and statistical techniques. *Earth and Planetary Science Letters* **302**, 154-162.

Hanghøj, K. (2005). Report on exploration activities in 2004 on Skaergaard license no. 2005/09. Internal report, Skaergaard Minerals., Corp, 51 pp, 1 EA: Geochemical analyses, core recovery, drill hole survey, 175 pp. (In archive of the Geological Survey of Denmark and Greenland, report GRF 21895; (available online at www.greenmin.gl).

Holness, M.B., Stripp, G., Humphreys, M.C.S., Veksler, I.V., Nielsen, T.F.D. & Tegner, C. (2011). Silicate liquid immiscibility within the crystal mush: late-stage magmatic microstructures in the Skaergaard intrusion, east Greenland. *Journal of Petrology* **52**, 175–222.

Holness, M.B., Vukmanovic, Z. & Mariani, E. (2017a). Assessing the role of compaction in the formation of adcumulates: a microstructural perspective. *Journal of Petrology* **58**, 643-673.

Holness, M.B., Tegner, C., Nielsen, T.F.D & Charlier, B. (2017b). The thickness of the mushy layer on the floor of the Skaergaard magma chamber at apatite saturation. *Journal of petrology* **58**, 909-932.

Holness, M.B., Nielsen, T.F.D, & Tegner, C. (2017c). The Skaergaard intrusion of east Greenland: Paradigms, problems and new perspectives. *Elements* **13***,* 391-396.

Holwell, D. & Keays, R.R. (2014). The formation of low-volume, high-tenor magmatic PGE-Au sulfide mineralisation in closed systems: evidence from precious and base metal geochemistry of the Platinova reef, Skaergaard Intrusion, East Greenland. *Economic Geology* **109**, 387-406.

Holwell, D.A., Keays, R.R, McDonald, I. & Williams, M.R. (2015). Extreme enrichment of Se, Te, PGE and Au in Cu sulfide microdroplets: evidence from LA-ICP-MS analysis of sulfidesin the Skaergaard Intrusion, east Greenland. *Contributions to Mineralogy and Petrology*, **170**, 53.

Holwell, D.A., Barnes, S.J., Le Vaillant, M., Keays, R.R., Fisher & L.A. Prasser, R. (2016). 3D textural evidence for the formation of ultra-high tenor precious metal bearing sulfide microdroplets in offset reefs: An extreme example from the Platinova Reef, Skaergaard Intrusion, Greenland *Lithos,* **256-257**, 55-74.

Irvine, T.N. (1970). Heat transfer during solidification of layered intrusions. I. sheets and sills. *Canadian Journal of Earth Science*, **7**: 1031-1061.

Irvine, T.N., Andersen, J.C.Ø., & Brooks, C.K. (1998). Included blocks (and blocks within blocks) in the Skaergaard Intrusion: geological relations and the origins of rhythmic modally graded layers. *Geological Society of America Bulletin* **110**, 1398-1447.

Keays, R.R. & Tegner, C. (2016) Magma Chamber Processes in the Formation of the Low-sulphide Magmatic Au–PGE Mineralization of the Platinova Reef in the Skaergaard Intrusion, East Greenland. *Journal of petrology* **56**, 2319-2340.

Kuo, C. S. (2007). The mineral industries of Denmark, the Faroe Islands, and Greenland. US Geological Survey: Mineral Yearbook **2005**, 8.1-8.4.

Latypov, R., Chistyakova, S. & Mukherjee,R. (2017). A Novel Hypothesis for Origin of Massive Chromitites in the Bushveld Igneous Complex. *Journal of petrology* **58**, 1899-1940.

Laznicka (2006). *Giant Metallic Deposits: Future Sources of Industrial Metals*. Berlin Heidelberg: Springer-Verlag, 732 pp.

Le Matire, R.W. (1982). Numerical Petrology: Statistical interpretation of geochemical data. Elsevier, pp 281.

McBirney, A. R. (1989). The Skaergaard Layered Series: 1. Structure and average compositions. *Journal of Petrology* **30**, 363-397.

McBirney, A. R. (1996). The Skaergaard Intrusion. In: Cawthorn,R. G. (ed.) *Layered Intrusions*. Elsevier, pp. 147–180.

McDonald A.M., Cabri L.J., Rudashevsky N.S., Stanley C.J., Rudashevsky V.N., Ross K.C. Nielsenite, $PdCu_3$, a new platinum group intermetallic mineral species from the Skaergaard intrusion, Greenland. *The Canadian Mineralogist* **46,** 709–716.

McKenzie, D. (2011) Compaction and crystallization in magma chambers: toward a model for the Skaergaard intrusion. *Journal of Petrology* **52**, 905-930.

Makovicky, E. (2002). Ternary and quaternary phase systems with PGE. In J.P. Cabri (ed.): *The geology, geochemistry, mineralogy and mineral beneficiation of platinum-group elements.* Montreal: Canadian Institute of Mining, Metallurgy and Petroleum, Montreal, 131-175.

Miller, J.D. & Andersen, J.C.O. (2002). Attributes of Skaergaard-Type PGE Reefs. In Boudreau, A. (ed.). *Extended abstracts, 9th internat. Platinum Conference*, 305-308.

Morse, S.A. (2011). The fractional latent heat of crystallizing magmas. *American Mineralogist*, **96**, 682-689.

Naldrett, A.J., 2011, Fundamentals of Magmatic Sulphide Deposits. *Reviews in Economic Geology* **17**, 1-50.

Nielsen, T.F.D. (2004). The shape and volume of the Skaergaard Intrusion, Greenland: implications for mass balance and bulk composition. *Journal of Petrology* **45**, 507-530.

Nielsen, T.F.D. (2016). In situ fractionation and inward migration of the solidification front in the Skaergaard intrusion, East Greenland. *Geological Survey of Denmark and Greenland Bulletin* **35**, 59–62.

Nielsen, T.F.D. & Bernstein, S. (2009). Chemical stratigraphy of the Triple Group and mineralization of the Skaergaard intrusion: insight in the crystallisation process. *AGU Fall meeting 2009, Abstract* **V21A**-1956.

Nielsen, T.F.D., Andersen, J.C.Ø. & Brooks, C.K. (2005). The Platinova Reef of the Skaergaard intrusion. In: Mungal, J.E (ed.) *Exploration for Platinum Group element deposits.* Ottawa: Mineralogical Association of Canada, Short Course **35**, 431-455.

Nielsen, T.F.D., Rasmussen, H., Rudashevsky, N.S., Kretser, Yu.L. & Rudashevsky, V.N. (2003a). PGE and sulphide phases of the precious metal mineralisation of the Skaergaard intrusion. Part 1: sample 90-23A, 807. *GEUS report* **2003/47**, 46 pp. (available online at www.greenmin.gl)

Nielsen, T.F.D., Rasmussen, H., Rudashevsky, N.S., Kretser, Yu.L. & Rudashevsky, V.N. (2003b). PGE and sulphide phases of the precious metal mineralisation of the Skaergaard intrusion. Part 2: sample 90-24, 1057. *GEUS report* **2003/48**, 83 pp. (available online at www.greenmin.gl)

Nielsen, T.F.D., Rasmussen, H., Rudashevsky, N.S., Kretser, Yu.L. & Rudashevsky, V.N. (2003c). PGE and sulphide phases of the precious metal mineralisation of the Skaergaard intrusion. Part 3: sample 90-18, 1010. *GEUS report* **2003/52**, 67 pp. (available online at www.greenmin.gl)

Nielsen, T.F.D., Rasmussen, H., Rudashevsky, N.S., Kretser, Yu.L. & Rudashevsky, V.N. (2003d). PGE and sulphide phases of the precious metal mineralisation of the Skaergaard intrusion. Part 4: sample 90-23A, 806. *GEUS report* **2003/53**, 40 pp. (available online at www.greenmin.gl)

Nielsen, T.F.D., Rasmussen, H., Rudashevsky, N.S., Kretser, Yu.L. & Rudashevsky, V.N. (2003e). PGE and sulphide phases of the precious metal mineralisation of the Skaergaard

intrusion. Part 5: sample 90-23A, 808. *GEUS report* **2003/54**, 37 pp. (available online at www.greenmin.gl)

Nielsen, T. F., Tegner, C., Thy, P., Fonseca, A .K.,Jakobsen, J. K., Kristensen, M., Simpson, J. A., Brooks, C., Kent, A. J., Peate, D. W. & Lesher, C. E. (2000). Retrieval of Platinova drill cores: a new Skaergaard initiative. *Eos Trans*. *AGU* **81** (48), Fall Meet, Suppl. abstract V21E-15

Nielsen, T.F.D., Olsen, S.D. & Stensgaard. B.M. (2009). Developing a 3-D model for the Skaergaard intrusion in East Greenland: constraints on structure, mineralization and petrogenetic models. *Geological Survey of Denmark and Greenland Bulletin* **17**, 61-64.

Nielsen, T.F.D., Andersen, J.C.Ø., Holness, M.B., Keiding, J.K., Rudashevsky, N.S., Rudashevsky, V.N., Salmonsen, L.P., Tegner, C. & Veksler, I.V. (2015). The Skaergaard PGE and gold deposit: the result of in situ fractionation, sulphide saturation, and magma chamber scale precious metal redistribution by immiscible Fe-rich malt. *Journal of Petrology* **56**, 1643-1976.

Pawlowsky-Glahn, V. & Egozcue, J.J. (2006) Compositional data and their analysis: an introduction. *Geological Society, London, Special Publications*, **264**, 1-10.

Prendergast, M.D. (2000). Layering and precious metals mineralization in the Rincón del Tigre complex, Eastern Bolivia. *Economic geology* **95**, 11-130.

Rudashevsky, N.S., McDonald, A.M., Cabri, L.J.,Nielsen, T.F.D., Stanley, C.J., Kretser, Yu.L., Rudashevsky, V.N. (2004). Skaergaaardite, PdCu, a new platinum group intermetallic mineral from the Skaergaard intrusion, Greenland, *Mineralogical Magazine* **68**, 615–632.

Rudashevsky, N.S. and Rudashevsky, V.N. (2005a). Gold, PGE, and sulphide phases of the precious metal mineralisation of the Skaergaard intrusion. Sample 90-24, 1018. Part 29, sample 90-24 1018. Unpublished GEUS report, 19pp plus tables and plates (available on request).

Rudashevsky, N.S. and Rudashevsky, V.N. (2005b). PGE, gold, and sulphide phases of the precious metal mineralisation of the Skaergaard intrusion. Sample 90-24, 1022. Part 28, sample 90-24 1022. Unpublished GEUS report, 21pp plus tables and plates (available on request).

Rudashevsky, N.S and Rudashevsky, V.N. (2006a). PGE, gold, and sulphide phases of the precious metal mineralisation of the Skaergaard intrusion. Sample 90-24, 1045N. Part 21,

sample 90-24 1045N, Unpublished GEUS report, 17pp plus tables and plates (available on request).

Rudashevsky, N.S. and Rudashevsky, V.N. (2006b). PGE, gold and sulphide phases of the precious metal mineralisation of the Skaergaard intrusion. Sample 90-24, 1034. Part 24, sample 90-24 1034. Unpublished GEUS report, 25pp plus tables and plates (available on request).

Rudashevsky, N.S., Kretser, Y.L., Rudashevsky, V.N. & Nielsen, T.F.D. (2009a). Gold, PGE and sulphide phases of the precious metal mineralisation of the Skaergaard intrusion. Part 7, sample 90-18 958. *GEUS report* **2009/68**, 16 pp plus tables and plates.

Rudashevsky, N.S., Kretser, Y.L., Rudashevsky, V.N. & Nielsen, T.F.D. (2009b). Gold, PGE and sulphide phases of the precious metal mineralisation of the Skaergaard intrusion. Part 6, sample 90-23A 798. *GEUS report* **2009/54**, 17 pp plus tables and plates.

Rudashevsky, N.S., Rudashevsky, V.N. & Nielsen, T.F.D. (2010a). Gold, PGE and sulphide phases of the precious metal mineralisation of the Skaergaard intrusion. Part 8, sample 90-18 972. *GEUS report* **2010/73**, 19 pp plus tables and plates.

Rudashevsky, N.S., Rudashevsky, V.N. & Nielsen, T.F.D. (2010b). Gold, PGE and sulphide phases of the precious metal mineralisation of the Skaergaard intrusion. Part 9, sample 90-18 978. *GEUS report* **2010/74**, 21 pp plus tables and plates (available online at www.greenmin.gl).

Rudashevsky, N.S., Rudashevsky, V.N. & Nielsen, T.F.D. (2010c). Gold, PGE and sulphide phases of the precious metal mineralisation of the Skaergaard intrusion. Part 10, sample 90-18 988. *GEUS report* **2010/85**, 16 pp plus tables and plates (available online at www.greenmin.gl).

Rudashevsky, N.S., Rudashevsky, V.N. & Nielsen, T.F.D. (2010d). Gold, PGE and sulphide phases of the precious metal mineralisation of the Skaergaard intrusion. Part 11, sample 90-24 1062. *GEUS report* **2010/138, 17** pp plus tables and plates (available online at www.greenmin.gl).

Rudashevsky, N.S., Rudashevsky, V.N. & Nielsen, T.F.D. (2012a). Gold, PGE and sulphide phases of the precious metal mineralisation of the Skaergaard intrusion. Part 12, sample 90-18 1001. *GEUS report* **2012/91,** 13 pp plus tables and plates (available online at www.greenmin.gl).

Rudashevsky, N.S., Rudashevsky, V.N. & Nielsen, T.F.D. (2012b). Gold, PGE and sulphide phases of the precious metal mineralisation of the Skaergaard intrusion. Part 13, sample 90-18 1012. *GEUS report* **2012/92,** 20 pp plus tables and plates (available online at www.greenmin.gl).

Rudashevsky, N.S., Rudashevsky, V.N. & Nielsen, T.F.D. (2012c). Gold, PGE and sulphide phases of the precious metal mineralisation of the Skaergaard intrusion. Part 14, sample 90-10 434, *GEUS report* **2012/93**, 19 pp plus tables and plates (available online at www.greenmin.gl).

Rudashevsky, N.S., Rudashevsky, V.N. & Nielsen, T.F.D. (2012d). Gold, PGE and sulphide phases of the precious metal mineralisation of the Skaergaard intrusion. Part 15, sample 90-10 443, *GEUS report* **2012/94**, 19 pp plus tables and plates (available online at www.greenmin.gl).

Rudashevsky, N.S., Rudashevsky, V.N. & Nielsen, T.F.D. (2012e). Gold, PGE and sulphide phases of the precious metal mineralisation of the Skaergaard intrusion. Part 16, sample 90-10 445, *GEUS report* **2012/95**, 16 pp plus tables and plates (available online at www.greenmin.gl).

Rudashevsky, N.S., Rudashevsky, V.N. & Nielsen, T.F.D. (2012f). Gold, PGE and sulphide phases of the precious metal mineralisation of the Skaergaard intrusion. Part 17, sample 90-24 1059. *GEUS report* **2012/96,** 17 pp plus tables and plates (available online at www.greenmin.gl).

Rudashevsky, N.S., Rudashevsky, V.N. & Nielsen, T.F.D. (2012g). Gold, PGE and sulphide phases of the precious metal mineralisation of the Skaergaard intrusion. Part 18, sample 90-24 1056. *GEUS report* **2012/97,** 20 pp plus tables and plates (available online at www.greenmin.gl).

Rudashevsky, N.S., Rudashevsky, V.N. & Nielsen, T.F.D. (2012h). Gold, PGE and sulphide phases of the precious metal mineralisation of the Skaergaard intrusion. Part 19, sample 90-24 1053 *GEUS report* **2012/98**, 15 pp plus tables and plates (available online at www.greenmin.gl).

Rudashevsky, N.S., Rudashevsky, V.N. & Nielsen, T.F.D. (2012i). Gold, PGE and sulphide phases of the precious metal mineralisation of the Skaergaard intrusion. Part 20, sample 90-24 1048. *GEUS report* **2012/104**, 20 pp plus tables and plates (available online at www.greenmin.gl).

Rudashevsky, N.S. Rudashevsky, V.N. Nielsen, T.F.D. & Shebanov, A.D. (2014) Au-Cu alloys and inter-metallides in Pd-Au ores of the Skaergaard massif. *Proceedings of the Russian Mineralogical Society* **143(4)**, 1-23.

Rudashevsky, N.S. Rudashevsky, V.N. & Nielsen, T.F.D. (2015). Intermetallides and alloys of copper and palladium in ores of the Skaergaard massif. *Proceedings of the Russian Mineralogical Society* **144(1)**, 30-53.

Salmonsen, L.-P. (2013). Petrology of the Upper Border Series of the Skaergaard intrusion. Ph.D thesis, Aarhus University, 96 pp.

Salmonsen, L.P. & Tegner, C. (2013). Crystallisation Sequence of the Upper Border Series of the Skaergaard Intrusion: Revised subdivision and implications for chamber-scale magma homogeneity. *Contributions to Mineralogy and Petrology* **165**, 1155-1171.

Svennevig, K. & Guarnieri, P. (2012). From 3D mapping to 3D modelling: a case study from the Skaergaard intrusion, southern East Greenland. *Geological Survey of Denmark and Greenland Bulletin* **26**, 57-60.

Tegner, C., Thy, P., Holness, M.B., Jakobsen, J.K & Lesher, C.E. (2009). Differentiation and compaction in the Skaergaard Intrusion. *Journal of Petrology* **50**, 813-840.

Turner, P.A. & Mosher, W. (1989). Report of 1988 field season: Skaergaard concession and East Greenland concession license. Platinova Resources Ltd/Corona Corporation Joint Venture, 71 pp. plus EA´es and maps (in archive of Geological Survey of Denmark and Greenland, GRF 20845; available online at www.greenmin.gl).

Ueki. K. & Iwamori, H. (2017). Geochemical differentiation processes for arc magma and the Sengan volcanic cluster, Northeastern Japan, constrained from principal component analysis. *Lithos* **290-291**, 60-75.

Vukmanovic, Z.; Holness, M. B.; Monks, K. & Andersen, J. C. Ø. (2018). The Skaergaard trough layering: sedimentation in a convecting magma chamber. *Contributions to Mineralogy and Petrology* **173**:43.

Wager, L.R. & Brown, G.M. (1968). *Layered Igneous Rocks*. Edinburgh and London: Oliver and Boyd, 588pp.

Watts, Griffis & McOuat Limited (1991). 1990 Skaergaard project, Platinova/Corona concession, East Greenland. Exploration report, 55 pp. and EA'es (in archive of the Geological Survey of Denmark and Greenland, GRF no. 20848, available online at www.greenmin.gl).

Wotzlaw, J.-F., Bindeman, I.N., Schaltegger, U., Brooks, C.K. & Naslund, H.R. (2012). High-resolution insights into episodes of crystallisation, hydrothermal alteration and remelting in the Skaergaard intrusive complex. *Earth and Planetary Science Letters* **355**, 199-212.

Figure captions

Fig.1: Geology of the Skaergaard intrusion: (a) Map with series (LS, MBS and UBS), zones of LS, collar locations for drill cores and the sampling site "Toe of Forbindelsesgletscher" (ToF), and the chip lines Midnat (Mn) and Middag (Md) Buttresses. Red star: position of the centre of the mineralisation used in Fig. 10; (b) E-W section through the intrusion with subdivisions in Fig. 1a, and (c) schematic representation of the correlation between zones and subzones of LS, MBS and UBS. After Nielsen *et al.* (2015) and Salmonsen &Tegner (2013).

Fig. 2: a) Western face of Wagertoppen (1277 m) with the three leucogabbro layers of Triple Group (TG). The layering is in the upper left disturbed by large blocks of gabbro assumed derived from the roof of the magma chamber. The layering drapes over the blocks of UBS sunk into the magma chamber (e.g., lower right; photo by M.B. Holness. b) Close-up of the north-western ridge of Wagertoppen (photo by J.C. Ø. Andersen) showing L1 and L2 of TG maintaining constant stratigraphic separation even in the most north-western exposures and the distinct layering of the zebra-banded zone the lower part of the image. Includes several leucogabbro blocks and rafts, some coherent and some smeared out parallel to the layering in the gabbroic host. Yellow vertical bars identify the macro-rhythmic layers (ML0-ML2.2) of the mineralised section of TG, each with a plagioclase rich top. Pd5 of the mineralisation is hosted in the upper metres of ML0, and Pd1 which host the main Au concentration in central parts of the intrusion is hosted in ML2.1.The section of MLs covered by the Midnat chipline (Turner and Mosher, 1989) is also shown.

Fig. 3. Examples of available elemental and density profiles through the Skaergaard PGE-Au Mineralisation (see Fig. 1a for locations). a) From left to right: in order of increasing distance from centre of the concentric mineralisation. Compositional profiles: PGE (Pd+Pt) in blue; Au in yellow; and Cu in red in a continuous 25-cm bulk rock profile in drill core 90-22 from the centre of the intrusion, 1-m continuous averages in drill core 90-17A located ~ 1150 m from the western margin, in drill core 90-23A located ~ 900 m from the eastern margin of the intrusion, and in the Middag chip line profile almost 5 km N of the centre of the mineralisation (se Fig. 1). Density profiles for drill cores 90-22 (centre) and 90-23A (margin) and in grey the logged elevation of leucolayers L0, and L1 and L2 of the Triple Group demonstrate the extreme

continuity of layering in host rocks as well as for the mineralisation levels and the upward migration relative to MLs of precious metals and Cu toward the supposed centre of the mineralisation. Details and sources for the plotted data can be found in Nielsen *et al.*, (2015) and EA therein. b) Cross section to scale after EA2 in Nielsen *et al.*, (2015) (see location in Fig. 1a) with elevations of intersects between drill cores and Pd5 (blue) and Pd1 (red) mineralisation levels and leucogabbro layer L3 (yellow) of Triple Group. Only drill cores for which all three markers are identified are included. In all others, one or more data points are lost in due to intersecting dykes. Mineralisation levels are concordant with the lithological layering in the 7000 m wide and >600 m deep bowl-shaped succession of macro-rhythmic layers (MLs) of upper Middle zone. Data for the compilation in can be found in EA1-3 in Nielsen *et al.* (2015).

Fig. 4: Schematic illustration of the structure of the precious metal mineralisation. The Pd-levels are concordant with the bowl-shape of the magmatic layering in the intrusion (Nielsen *et al.*, 2015, EA2). The circular structure of the mineralisation is based on modelling in Watts, Griffis and McOuat (1991), Andersen *et al.*, (1998), Nielsen *et al.*, (2005) and is idealised relative to the actual and more irregular structure. The colour change from blue to yellow symbolizes the lateral variation from PGE-rich to Au and Cu rich in mineralisation levels.

Fig. 5: Correlation between mineralisation levels, macro-rhythmic layers (MLs) of the host gabbros, and subdivision of the mineralisation as developed in the geographical centre of the multi-layered mineralisation (drill core 90-22). The subdivision of the gabbros into macro-rhythmic layers follows the principles in Nielsen *et al.* (2015, see also text for details). Left: the density profile is divided into MLs (centre) on the basis of the midpoint of marked increases in density, i.e., half way between the low density top of a lower ML and the density high near the base of the overlying ML. Grey sections identifies ilmenite rich intervals occurring at regular intervals but with no apparent correlation to the layering in MLs (see Nielsen *et al.*, 2015). Right: Mineralisation levels Pd6 and Pd5 in ML0, Pd4a,b in ML1.1, , Pd3a,b in ML1.2, , Pd2a,b in ML2, and Pd1 and Pd1/Au in ML2. Geochemical subdivision of the mineralisation into LPGEM, UPGEM, UAuM and CuM in centre column. The Au-rich combined Pd1 and Pd1/Au mineralisation levels have an average of 2.1 g/t precious metals over 3.6 m in drill core 90-22.

Fig. 6: Variation in PGE (Pd+Pt) and Au in drill cores 89-09, 89-09A and 89-09B from the central parts of the mineralisation. Data from Turner & Mosher (1990). Drill core 89-09 was wedged twice to produce three neighbouring cores (Figs 6a-c) through the mineralised gabbros The elemental profiles for PGE are very similar in all three cores, whereas the details of the uppermost Au-rich mineralisation (Figs 6d-f) varies significantly, despite having very similar grade times width numbers (g*w; average grade in grams/ton times the width or height of stratigraphic interval in metres; Table 2). The unconstrained distribution of gold is on basis of petrographic observations (Godel *et al.*, 2014) argued to be due to local and late redistribution (see text for further explanations).

Fig. 7: The volumetricly most important groups of precious metal minerals and phase encountered in samples from drill cores and bulk samples. Sulphide minerals vysotskite and vasilite dominate near the Archaean basement to the west, the plumbides and arsenides near basalts to the east, and Cu,PGE) alloys and minerals including skaergaardite (PdCu) dominate in the central parts of the intrusion. Au-rich paragenesis are dominated by tetra-auricupride (AuCu) and unnamed Au_3Cu. All data and information on methodes and sample can found in Table 4, EA5-12.

Fig. 8: Variation in total content of precious metals in "grade x width" numbers (g*w; average grade in grams/ton times the width or height of the stratigraphic interval in metres) in a section across the intrusion (Table 6). Circles: (Pd+Pt) in the 5 meters of drill core with the highest Pd+Pt in the Pd5 mineralisation level (potential ore horizon); diamonds: (Pd+Pt) in LPGEM (ML0 and ML1.1), triangles: (Pd+Pt) in the bulk mineralisation from a lower cut off at Pd6 to an upper cut below off above Pd1 of 100 ppb, and squares: (Pd+Pt+Au) for the bulk mineralisation (Ml0 to ML2.1). Blue: Platinova Resources A/S drill cores (Watts, Griffis and McOuat, 1991), red: Skaergaard Minerals Corporation (Hanghøj, 2005), and green: Holwell and Keays (2014). Open symbols: Low totals in drill cores 04-30, 89-03, -04, -06 north of the section and low in 90-18 south of the section. Further explanations in text.

Fig. 9: Au (g*w)-numbers (average grade in grams/ton times the width or height in metres) in a profile across the intrusion as compiled from base to top of the mineralisation and in the Pd5 mineralisation level. Orange: Au (g*w) in the 5-meter section in Pd5 with the highest (Pd+Pt) of the Pd5 mineralisation level (potential ore horizon, Table 6). Yellow: All Au in the mineralisation from <100 ppb below Pd6 (ML0) to <100 ppb above Pd1/Au (ML2.1). Red: Au

(g*w) number for sections through the entire mineralised succession of gabbro in drill cores from the margins of the intrusion. They provide an approximation to the average Au accumulated the mushy floor of the magma chamber and available for redistribution up macro-MLs. See text for further explanations. Fig. 10: Bulk precious metal contents as in Fig. 8, but plotted relative to an assumed geographical centre for the mineralisation (topographic point 666 on lower Basistoppen, see text for details, data in Table 6n). Blue: Watts Griffis and McOuat (1991), red: Hanghøj (2005) and green: Holwell & Keays (2014). Open symbols are (g*w; average grade in grams/ton times the width or height in metres) and ratios of precious metals in drill cores from the W-margin of the intrusion. Left column:(g*w) number from a lower cut off at <100 ppb below Pd6 to an upper cut off at <100 ppb above Pd1; centre column:(g*w) for LPGEM that (Nielsen *et al.* (2015) argued to have formed while precious metal were supplied from bulk magma; and right column: 5-meter section in Pd5 with the highest (Pd+Pt) of the Pd5 mineralisation level (potential ore horizon). For all are shown (Pd+Pt), (Pd+Pt+Au), and Pd/Pt, Au/Pt and Au/Pd ratios. As in Fig. 8, the lower centre of the mineralisation is relatively depleted in PGE and especially in Au (see also Fig. 9), whereas the upper central parts are enriched (see text for further descriptions and discussions). The mineralisation is not perfectly concentric and the open symbol data at 2500 m should be compared to the samples at the E-margin at 3500 to 4000 m. Data in Holwell *et al.* (2016) have been omitted as they give no Pt values.

Fig. 11: Relative Cu depletion in the geographic centre of the mineralisation due to dissolution of sulphide melt hosted in immiscible droplets. The shown 12-meter section in ML0 includes the main concentration of PGE (Pd5 /Pd-zone) and below Pd6 (subzone). Blue: drill cores from the E-margin incl. 90-23A, 04-34, 08-35A, and 11-57 green: drill cores from the W-margin incl. 04-30 and 90-14; orange: drill cores from the SW-part of the intrusion incl. 90-22 and 90-18 and red: drill cores from central parts incl. 04-32, 04-33, 11-53 and 90-24;; and ; all data in Table 7.

Fig. 12: Standardized loadings of the elements considered onto: (a) principal component 1 (PC1), (b) principal component 2 (PC2), and (c) principal component 3 (PC3).

Fig. 13: Fe as Fe_2O_3 wt % up the MLs of the Skaergaard mineralisation. Blue: central drill core 90-22, red: margin drill core 08-35A. The variations overlap and demonstrate that MLs maintain near constant thickness across the intrusion. Black column: the precious metal mineralised section of drill core 08-35A from near the margin of the intrusion in ML0 and ML1.1 in; grey column: mineralised ML0 to ML2.1 in drill core 90-22 in the centre of the mineralisation. Upper

golden field: the Au rich section in 90-22 at 0.7 ppm cut-off and green field: the Pd1 peak. The combined average is 2.1 g/t over 3.6 m (grade x width: 7.56). The lower golden field: the Au rich interval in drill core 08-35A (Holwell *et al.*, 2016) with an average of 2.2 g/t over 0.8 m (grade x width: 1.76). Depth in drill core 90-22 (Bernstein & Nielsen, 2004) data is calibrated to 08-35A by subtraction of 706 meter.

Fig. 14: Correlation between FeO* (FeO total) and P_2O_5 (wt %) in the continuous 25-cm sample profile from the base of the mineralisation below Pd6 to the Cu-rich gabbros above the precious metal rich mineralisation levels in drill core 90-22. Red: all samples (# 16) related to the gold-bearing Pd1 and Au/Pd1 mineralisation levels and sections of core with transgressive and late felsic veins. Blue: all other samples (# 243) in the profile demonstrate a negative correlation between FeO* and P_2O_5.

Fig. 15: Thin section views of mineralised gabbros in the Skaergaard mineralisation in drill core 90-22: (a) Pd5, peak of main PGE mineralisation level (1033.25m), and (b) Pd1, base of main Au-mineralised interval (993.5 to 990 m) showing extensive-late magmatic recrystallisation and alteration of clinopyroxene. Dissolution of plagioclase (greyish tones) and clinopyroxene (vivid colours) of the liquidus paragenesis and crystallisation of rim, and symplectites between late crystallised masses of FeTi-oxides (black) and the liquidus paragenesis are common to both mineralisation levels. Further descriptions in Holness *et al.* (2011) and in Nielsen *et al.* (2015).

Table Captions

Table 1: Stratigraphic elevation of mineralisation levels and bases of macrorhythmic layers across the intrusion and relative to elevation of Pd5.

Table 2. Table 2. Grade times width numbers (g*w) for the gold-peak in drill cores 89-09, 89-09A and 89-09B

Table 3: Identified PGE and Au native elements, minerals, unnamed minerals, intermetallic compounds and alloys of the PGE-Au mineralisation of the Skaergaard intrusion. Alloys are identified by their dominant elements in decreasing order.

Table 4: Summary of precious metal mineralogy of the Skaergaard PGE-Au mineralisation in vol. % of the precious metal paragenesis in individual samples. Comparisons and more detailed data in EA5-EA12.

Table 5: Stratigraphic variation in relative importance of precious metal mineral groups in Pd5 in drill cores 90-23A and 90-10 from near the E and W margins, respectively. Each sample collects t a 1-metre intervat inn the drill core.

Table 6. Grade times width* for Pd, Pt and Au in Skaergaard PGE-Au Mineralisation

Table 7. Bulk rock ((Pd+Pt+Au)/Cu)*1000 ratios in Pd5 relative to peak concentration (1-m averages).

Table 8: Summary of the first six principal components from the PCA.

Suplementary data

Electronic Appendix 1, Nielsen et al.

Correlation of Pd-levels and peaks (Pd+Pt in ppb) from west to east across the Skaergaard intrusion. Correlations are based on easily identified and at very low concentrations in logarithmic plots observed elemental peaks. The thirteen drill cores were selected because assay data as well as density data is availavle for all. In all cases is the vertical scale set to 0 meters at the Pd5 peak. Purple: Pd5; blue: Pd4a (upper) and Pd4b (lower peak); green: Pd3a (upper) and Pd3b (lower); orange: Pd2b; yellow: Pd2a and red: Pd1. Minor corrections of true stratigraphic scales due to faults and intersecting dykes in accordance with EA3 of Nielsen et al. (2015).

Electronic Appendix 2, Nielsen et al.

Correlation between PGE anomalies in the fully developed mineralisation (drill core 90-22) and assay profiles in drill cores from near the margins of the intrusion. Note that the scale for the concentrations of PGE is logarithmic in order to highlight low concentration anomalies. Pd5 is used as marker horizon (0 metres) and all elevations are relative to that peak. Note also that Pd1 and Pd1/Au peaks are readily identified and maintain near-constant elevations above Pd5 at concentrations of 10-100 ppb even to the margins of the intrusion.

Electronic Appendix 3, Nielsen et al.:

Correlation of density anomalies in Triple Group based on samples collected at 1 m intervals. Samples were weight in air and water for calculation of the density. Gaps in the measurements are due to intersecting dykes. Density heights as well as lows are correlated. The density profiles are lined up at the density low of L0. L1 is located ~20 meters, L2 ~ 40 metres and L3

~100 m above L0 across. The stratigraphic separation between L-layers is near constant across the intrusion from the west to the east margins (app. 7 km).

Electronic Appendix 4, Nielsen et al.:

Gold anomalies (orange) plotted on top elemental variation in Pd+Pt from EA1. All data in ppb. In all cases are gold peaks located in or marginally over a corresponding PGE peak. In no case is gold found to peak between peaks defined by PGE. Some drill cores (89-08 and 90-18) have two gold peaks separated by more than 10 metres with no more that traces of gold in between. The uppermost gold peak may be double due to accumulation of gold caused by sulphide saturation as well as deposition of gold along grain boundaries from mobile and residual mush melts (see Fig. 6 and text).

Electronic Appendix 5, Nielsen et al.:

Distribution of samples from the Skaergaard PGE-Au mineralisation that were used for the investigation of the precious metal mineral parageneses of the mineralisation

Schematic illustration of the distribution of samples in the Skaergaard PGE-Au Mineralisation relative to the geographical centre of the deposit. Peaks identify the mineralisation levels from which the samples were taken Columns to the right provide the precious metal 1-metre grades and depths (= # of the samples) in the given drill core or bulk sample. The investigated samples (purple) are shown from left to right with decreasing relative distance from the centre. The uncoloured boxes highlight the diachronous transition from the PGE- and Au-rich part of the mineralisation (LPGEM + UPGEM) to the Cu-rich gabbros (CuM) above the Au-rich mineralisation levels, irrespectively of their stratigraphic elevation in the layered gabbros.

Electronic Appendix 6, Nielsen et al.

PGE and Au mineralogy of macrorhythmic layer ML0.

Pd6 and Pd5 levels.

Electronic Appendix 7, Nielsen et al.

PGE and Au mineralogy of macrorhythmic layer ML1.1.

Pd4a and Pd4b levels.

Electronic Appendix 8, Nielsen et al.

PGE and Au mineralogy of macrorhythmic layer ML1.2.

Pd3a and Pd3b levels.

Electronic Appendix 9, Nielsen et al.

PGE and Au mineralogy of macrorhythmic layer ML2.

Pd2a and Pd2b levels.

Electronic Appendix 10, Nielsen et al.:

PGE and Au mineralogy of macrorhythmic layer ML2.1.

Pd1 and Pd1/Au levels.

Electronic Appendix 11, Nielsen et al.:

PGE and Au mineralogy of macrorhythmic layer ML2.2.

Pd1 and Pd1/Au levels.

Electronic Appendix 12, Nielsen et al.

Summary of precious metal mineralogy in Skaergaard mineralisation including data from Holwell et al. (2016).

Electronic Appendix 13, Nielsen et al.

Continuous profile in drill core 90-22. Density, major element, precious metal and trace element compositions.

Electronic Appendix 14, Nielsen et al.

Methods and results of Principal Component Analysis (PCA).

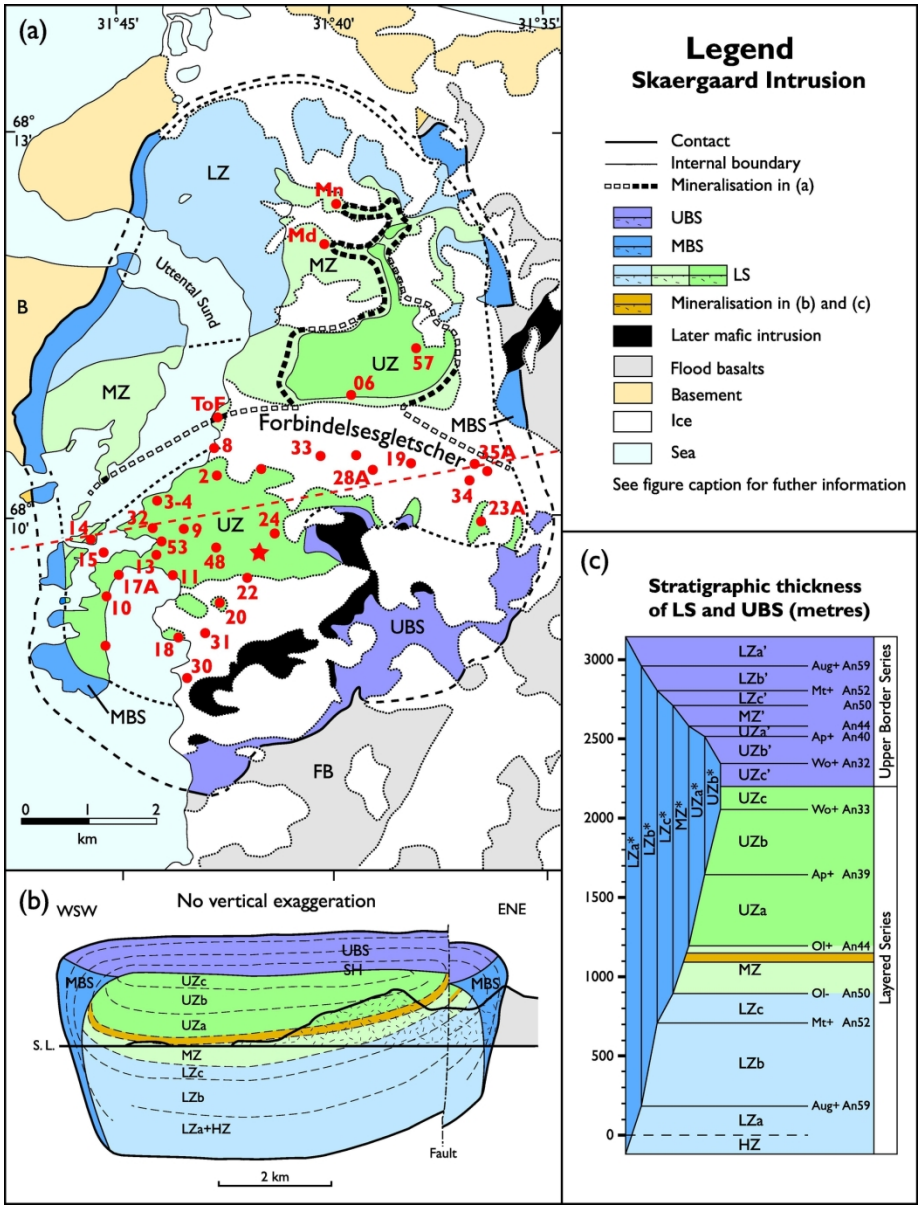

Fig. 1

161x212mm (300 x 300 DPI)

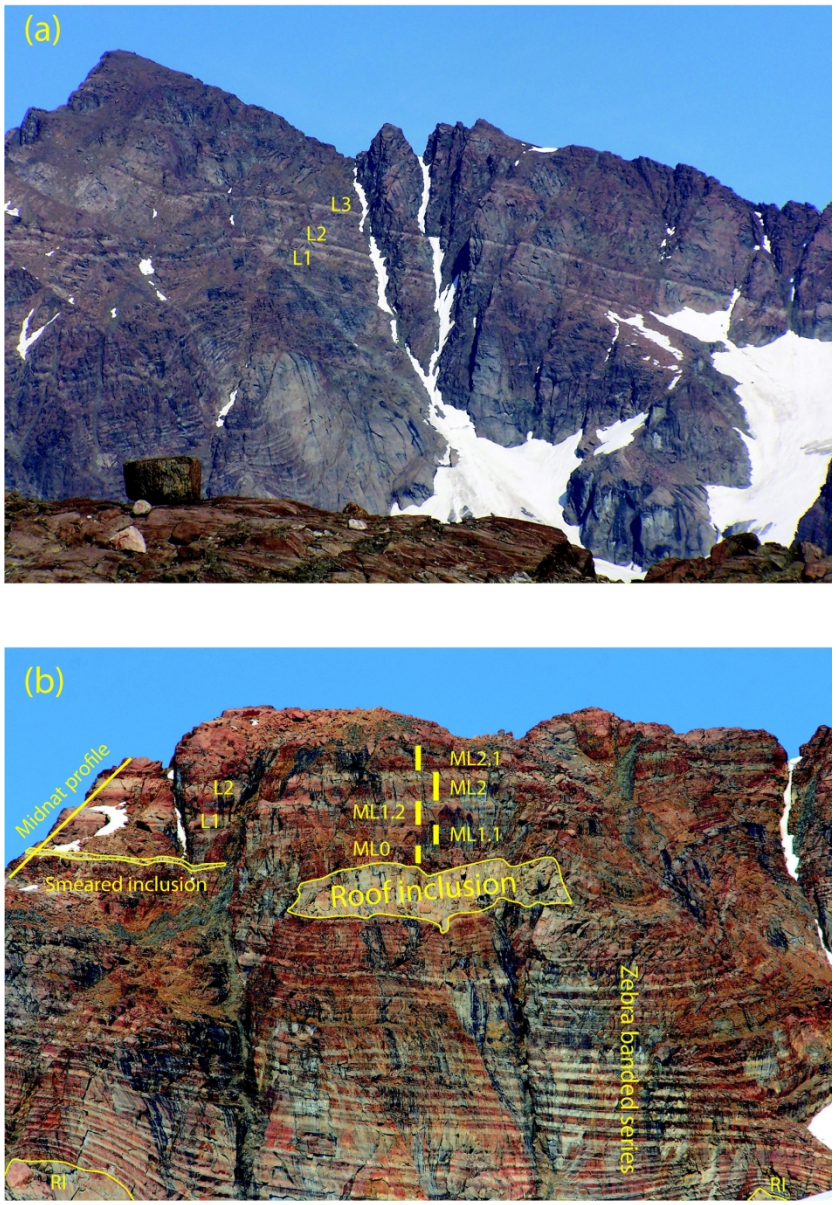

Fig. 2

165x239mm (300 x 300 DPI)

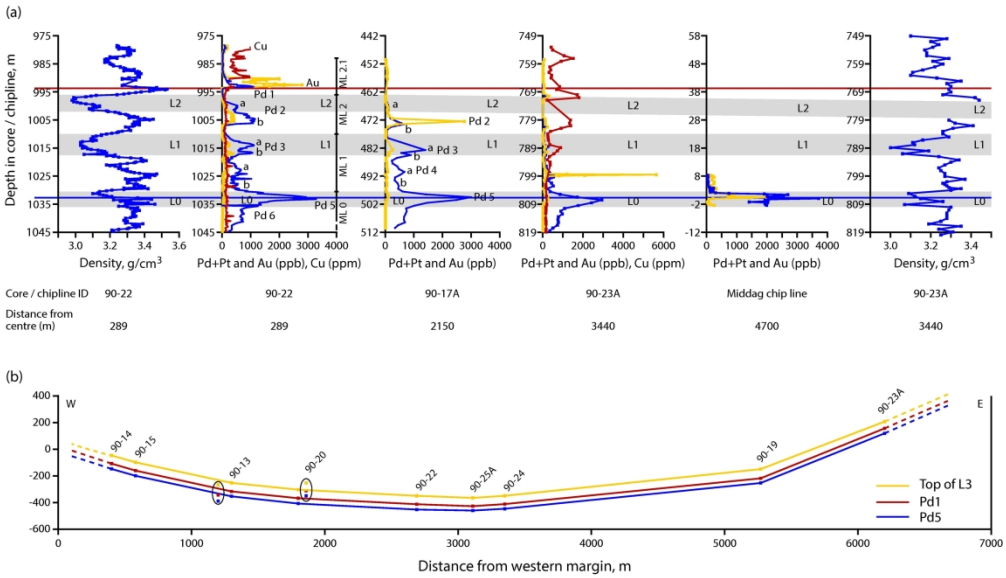

Fig. 3

228x200mm (300 x 300 DPI)

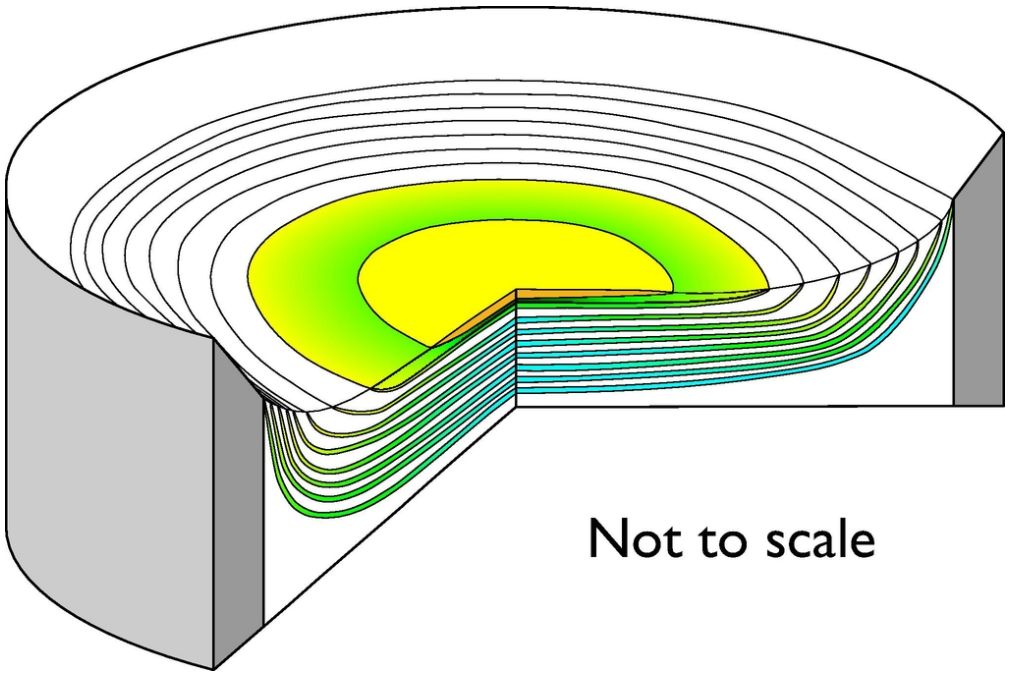

Fig. 4

86x57mm (300 x 300 DPI)

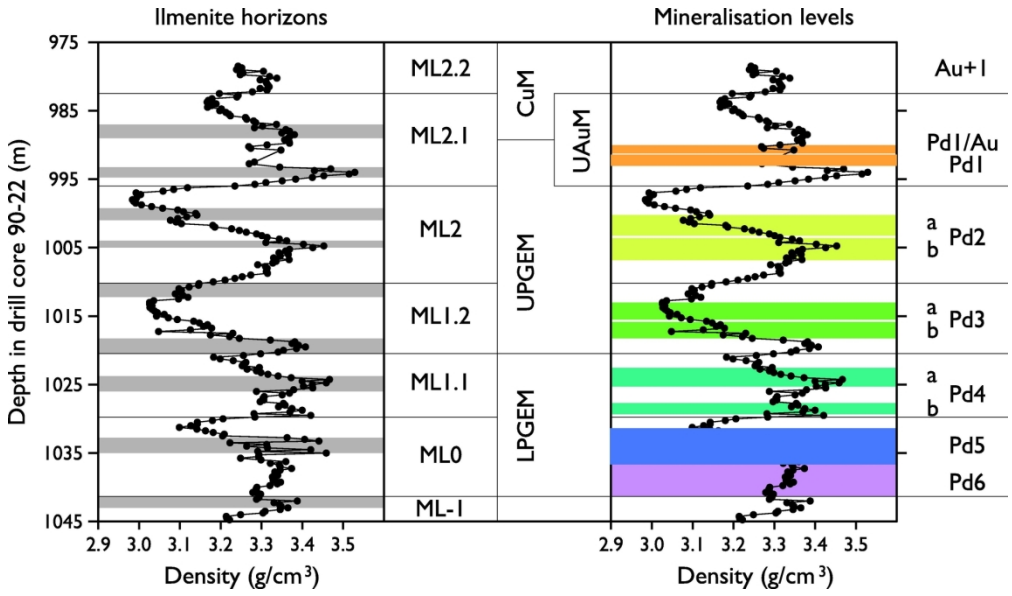

Fig. 5

174x101mm (300 x 300 DPI)

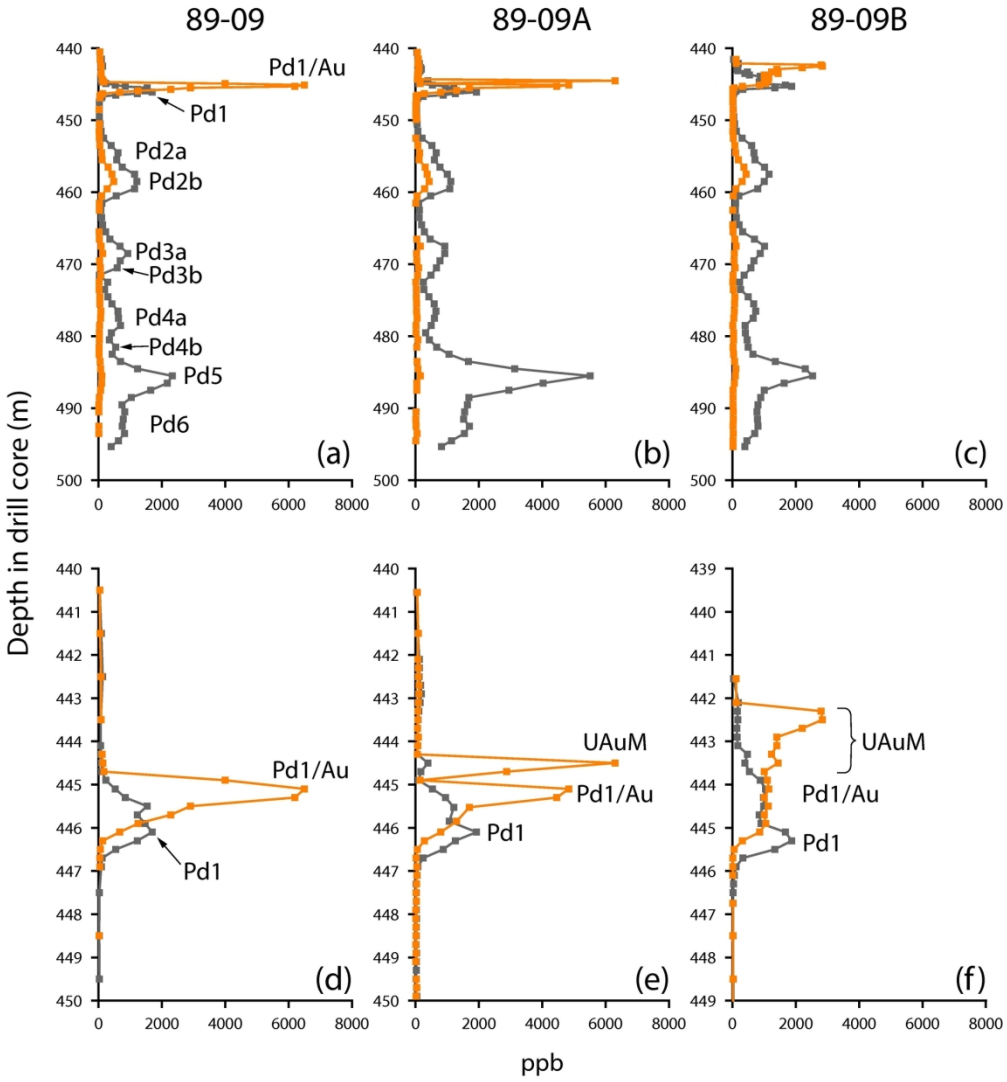

Fig. 6

168x180mm (300 x 300 DPI)

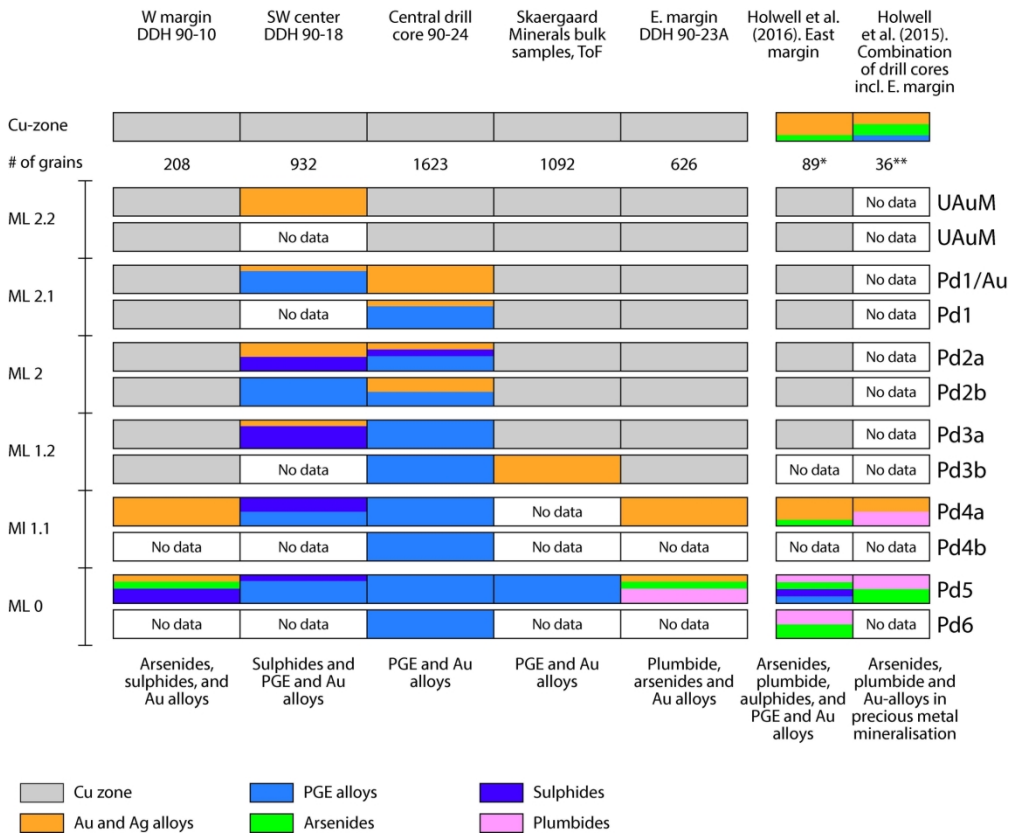

Fig. 7

182x150mm (300 x 300 DPI)

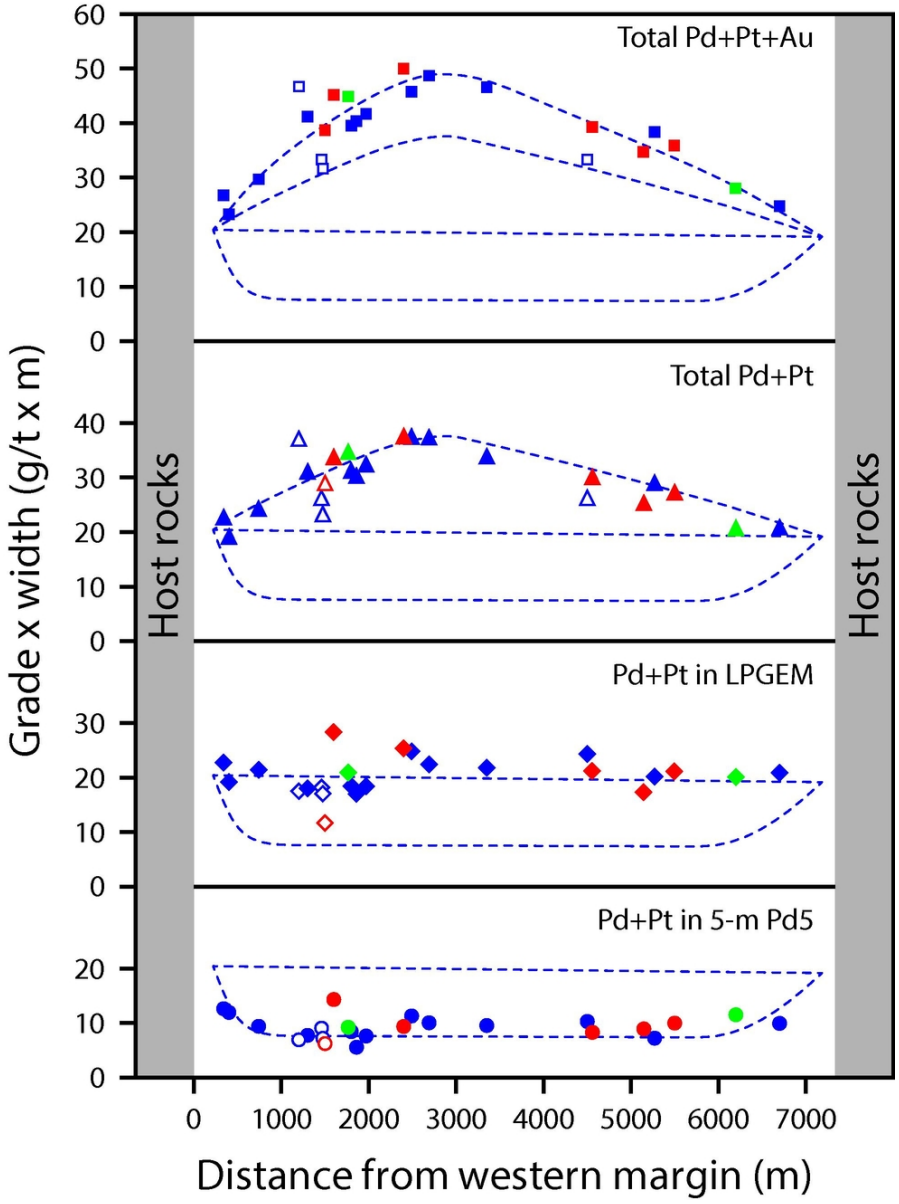

Fig. 8

83x112mm (300 x 300 DPI)

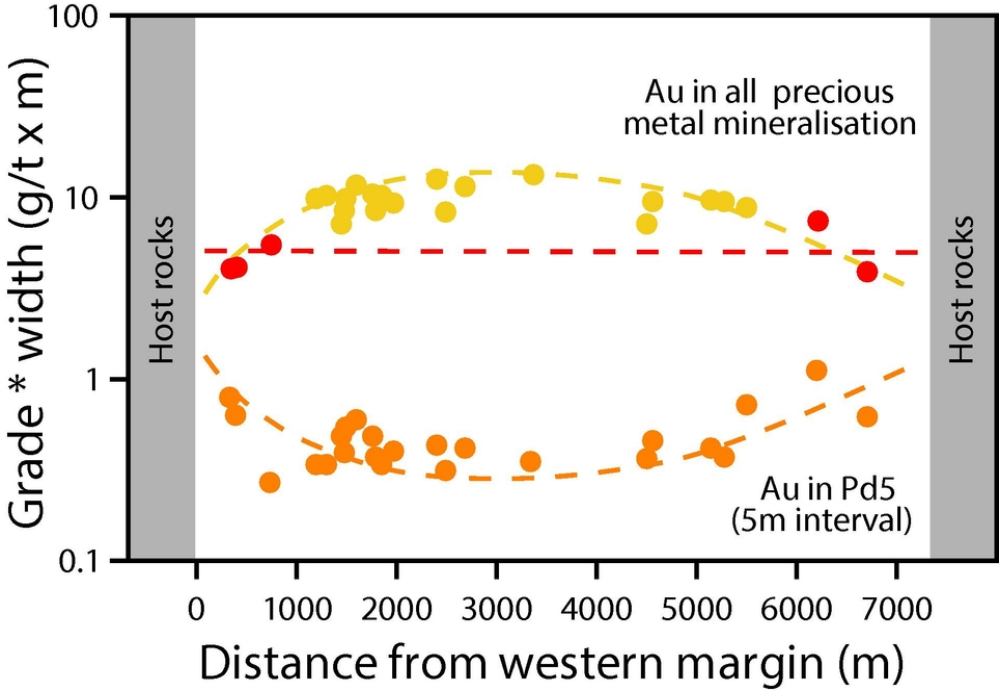

Fig. 9

81x56mm (300 x 300 DPI)

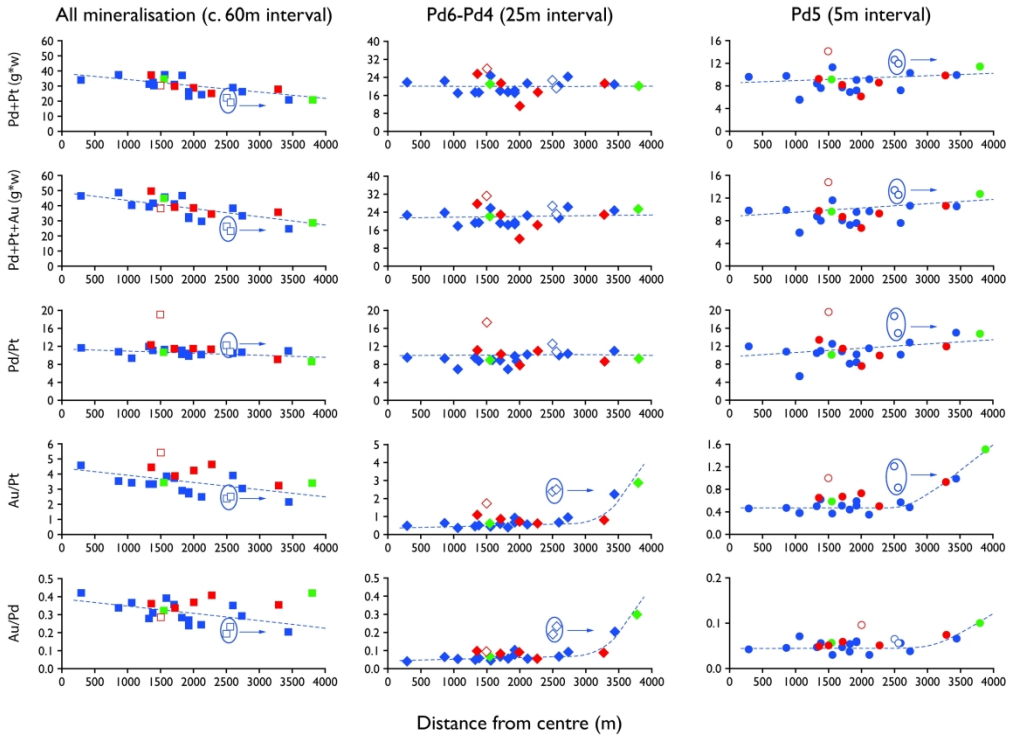

Fig. 10

282x206mm (300 x 300 DPI)

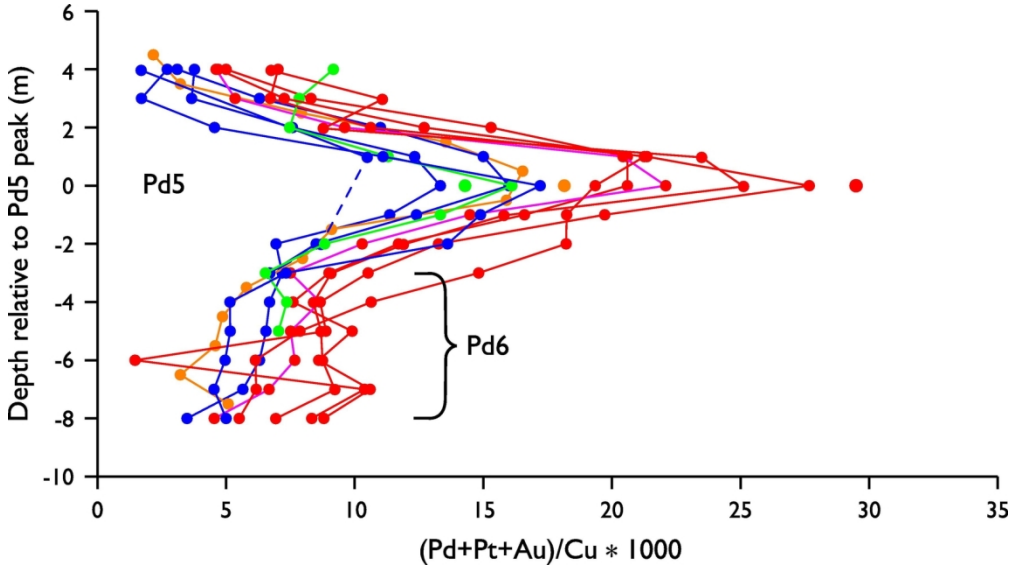

Fig. 11

149x83mm (300 x 300 DPI)

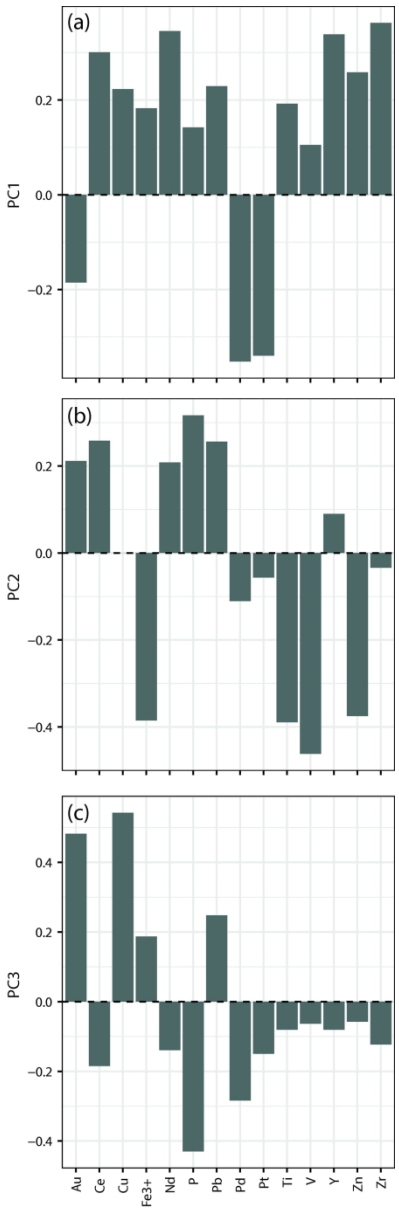

Fig. 12

90x278mm (300 x 300 DPI)

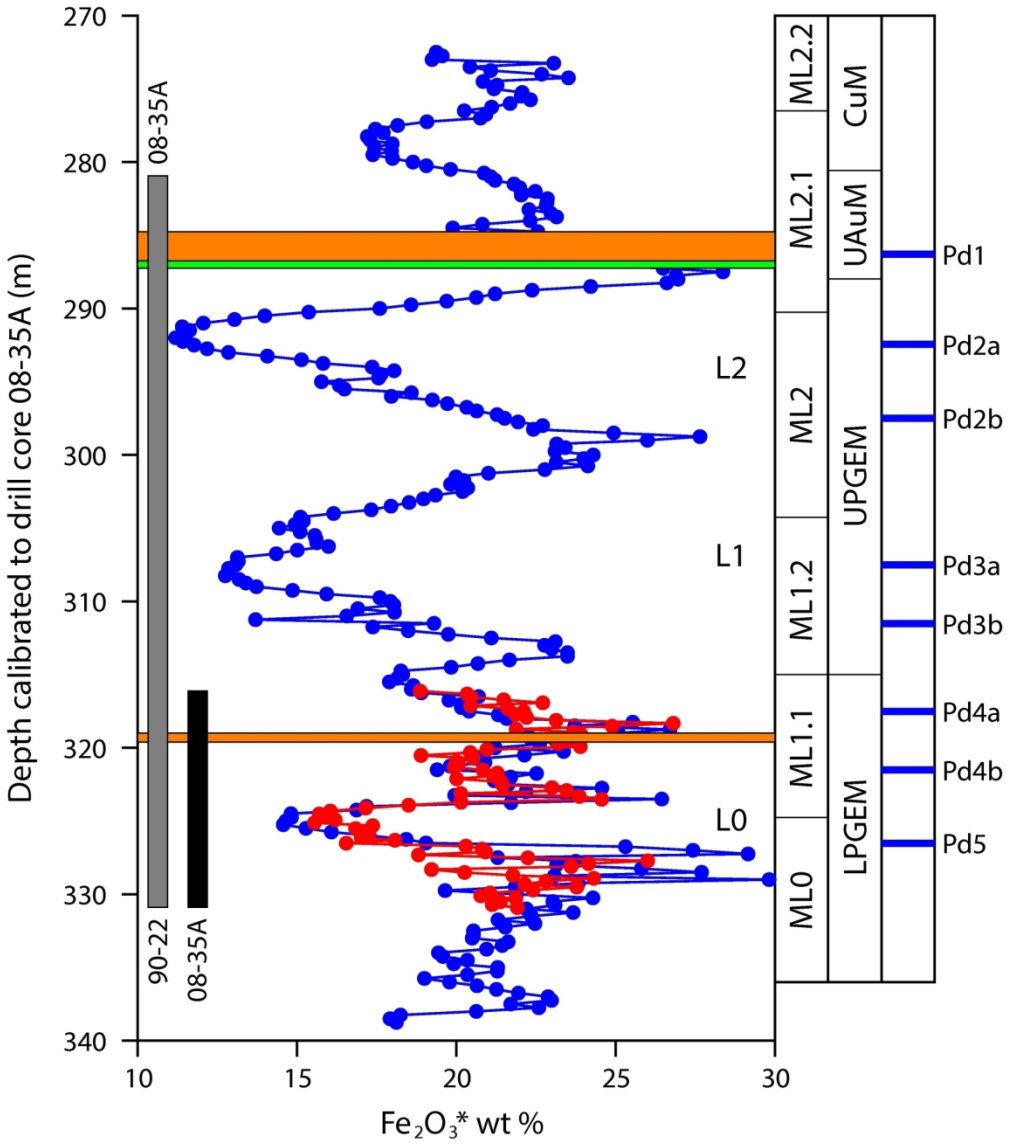

Fig. 13

150x171mm (300 x 300 DPI)

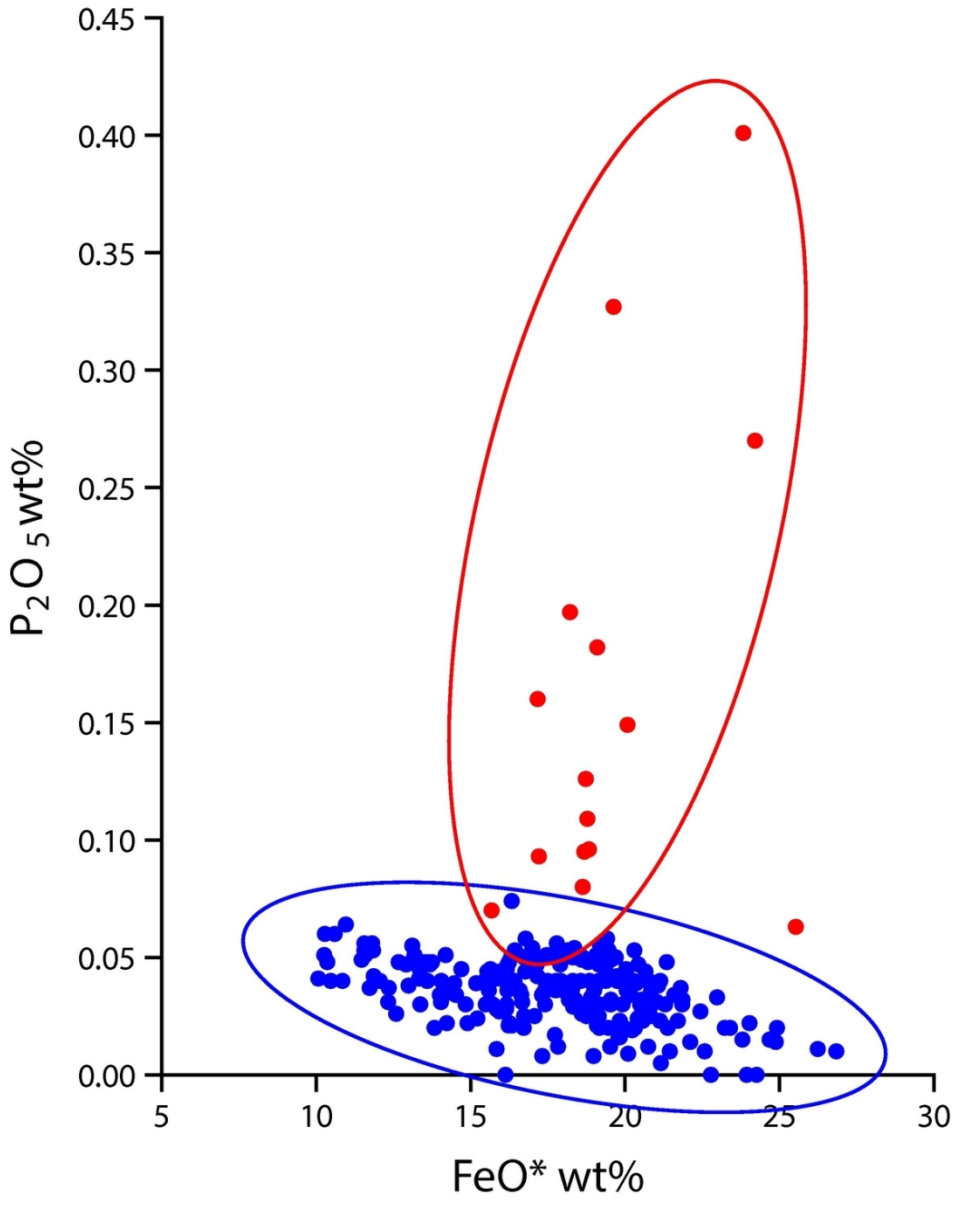

Fig. 14

100x126mm (300 x 300 DPI)

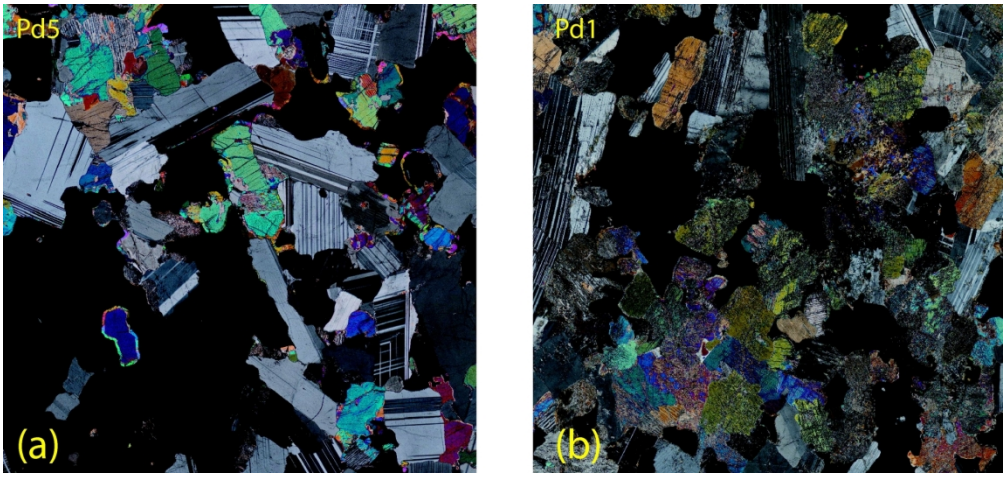

Fig. 15

175x82mm (300 x 300 DPI)

Table 1: Stratigraphic elevation of mineralisation levels and bases of macrorhythmic layers across the intrusion and relative to elevation of Pd5.

ML2.2	base	50.75
Pd/Au	peak	42.25
Pd1	peak	40.25
ML2.1	base	37.00
Pd2a	peak	32.50
Pd2b	peak	27.75
ML 2	base	23.00
Pd3a	peak	18.75
Pd3b	peak	16.50
ML1.2	base	12.25
Pd4a	peak	10.50
Pd4b	peak	5.50
ML1.1	base	2.50
Pd5.2*	peak	0.75
Pd5.1*	peak	0.00
ML0	base	-8.75

Based on 1-metre assays, logs and density profiles in 41 drill cores. Elevations relative to Pd5 are compiled in EA 1 and 3 in Nielsen et al. (2015).
* The Pd5 peak is, were resolution allows, divided in an upper and a lower maxima.

Table 2. Grade times width numbers (g*w) for the gold-peak in drill cores 89-09, 89-09A and 89-09B

Drill core	from (m)	to (m)	width (m)	Au av. ppb	PGE av. ppb	Au av. ppm	PGE av. ppm	PGE+Au g*w
4m interval								
89-9	443.0	447.0	4.0	1311	511	1.3	0.5	7.2
89-9A	443.4	447.0	4.0	1229	495	1.2	0.5	6.8
89-9B	442.0	446.0	4.0	1106	666	1.1	0.7	7.2
0.7 g/t cut off*								
89-9	444.8	446.4	1.6	2992	1093	3.0	1.1	6.6
89-9A	444.4	446.6	2.2	2277	848	2.3	0.9	7.0
89-9B	442.2	445.6	3.4	1293	747	1.3	0.7	6.8

* g*w; average grade in grams/ton of given stratigraphic interval multiplied by its height in meters.
** Cut off based on (Pd+Pt+Au). Data from Watts, Griffis and McOuat Ltd. (1991).

Table 3: Identified PGE and Au native elements, minerals, unnamed minerals, intermetallic compounds and alloys of the PGE-Au mineralisation of the Skaergaard intrusion. Alloys are identified by their dominant elements in decreasing order.

Native elements		**Minerals continued**	Formula	**Unnammed minerals**	**Alloys**	**alloys continued**
Native Ag	Ag	Majakite	PdNiAs	Au_3Ag	(Au,Ag,Cu)	(Pd,Au,Ag,Cu)
Native Pd	Pd	Merenskyite	$Pd(Te,Pb)_2$	Au_3Cu	(Au,Ag,Cu)	(Pd,Cu,As,Sb)
Native tellurium	Te	Naldrettite	Pd_2Sb	$(Cu,Pd)_{17}S_6$	(Au,Cu,Ag)	(Pd,Cu,Au,Pt)
		Nielsenite	$(Pd,Pt,Au)Cu_3$	$(Pd,Au)_7(Ni,Cu)_{11}Pb_2$	(Au,Cu,Ag)	(Pd,Cu,Pb)
Minerals	**Standart formula**	Palladoarsenide	$PdAs_2$	$(Pd,Au)_3(Cu,Fe)_6S_3(Te,Sn)_2$	(Au,Ag)	(Pd,Cu,Pb)
Acantite	Ag_2S	Palarstanide	$Pd_5(As,Sn)_2$	$AuPdCu_2$	(Au,Ag,Cu,Pd)	(Pd,Cu,Sn)
Arsenopalladinite	$Pd_8As_{2.5}Sb_{0.5}$	Polybasite	$(Ag,Cu)_{16}Sb_2S_{11}$	$(Pd,Ag)_2Te$	(Au,Cu)	(Pd,Ge,Cu)
Atokite	Pd_3Sn	Skaergaardite	PdCu	Pd_3Ag_2S	(Au,Cu,Fe)	(Pd,Pb,Cu)
Auricupride	Au_3Cu	Sopcheite	$Ag_4Pd_3Te_4$	Pd_3S	(Au,Cu,Pd)	(Pd,Pb,Cu,Sn,Te)
Bogdanovite	$(Au,Te,Pb)_3(Cu,Fe).$	Sperrylite	$PtAs_2$	$(Pt,Pd)Cu_3$	(Au,Cu,Pd,Ag)	(Pd,Pt,Cu)
Braggite	(Pt,Pd)S	Stefanite	Ag_5SbS_4	$(Au,Pd)_3(Cu,Fe)$	(Au,Pd,Cu,Pt,Ag)	(Pd,Sn,Cu)
Cabriite	Pd_2SnCu	Telargpalite	$(Pd,Ag)_{3+x}Te$	$(Cu,Pt,Pd)_3S_3$	(Au.Pd)Cu	(Pd,Te,As)
Electrum	(Au,Ag)	Telluropalladinite	Pd_9Te_4	$(Pd,Ag,Cu)_5S$	(AuCu,Ag)	(Pt,Cr,Pd)
Froodite	$PdBi_2$	Tetra auricupride	AuCu	$Pd_2(Cu,Fe)TeBi$	(Cu,Au)	(Pt,Cu,Fe)
Guanglinite	$Pd_3As.$	Tetraferriplatinum	PtFe	$(Au,Pd)_3(Cu,Fe)$	(Au,Cu, Pd)	(Pt,Cu,Fe,Pd)
Hessite	Ag_2Te	Tulameenite	$PtFe_{0.5}Cu_{0.5}$	$(Pd,Hg,Ag)_{2+x}S$	(Cu,Au,Ni,Zn)	(Pt,Fe,Cu)
Hongshite	PtCu	Vasilite	$Pd_{16}S_7$	Pd_3Ag_2S	(Cu,Pd,Pt)	(Pt,Fe,Pd)
Isomertiete	$Pd_{11}Sb_2As_2$	Vincentite	Pd_3As	$(Au,Pd)_3(Cu,Fe)$	(Cu,Pt,Pd)	(Pt,Fe,Pd,Cu)
Keithconnite	Pd3,xTe(0.14<x<0.43)	Vysotskite	PdS	$(Pd,Ag,Cd,Cu,Tl)_4S$	(Cu,Pt,Pd)	(Pt,Pd,As)
Kotulskite	PdTe	Zvyagintsevite	Pd_3Pb	$(Pd,Ag,Cu)_6S$	(Pd,Ag,Cu)	(Pt,Pd,Fe)
				$Pd_{11}As_2Sn_2$		

Sources:Bird et al., 1991; Nielsen et al, 2003_{a-e}, 2005, 2015; Cabri, 2004; Rudashevsky et al., 2005_{a-b}, 2006_{a-b}, 2009, $2010_{a-d,}$ 2012_{a-i}, 2007, 2009, 2014 2015; Holwell et al., 2015 and 2016

Table 4: Summary of precious metal mineralogy of the Skaergaard PGE-Au mineralisation in volume % of the precious metal paragenesis in individual samples. Comparisons and more detailed data in EA5-EA12

		West Margin	South center (SW core)		*Center*		Half way to Centre	East margin
		Drill core 90-10 Upper mineralisation level	Drill core 90-18 Lower mineralisation level	Drill core 90-18 Upper mineralisation level	*Drill core 90-24 Lower mineralisation level*	*Drill core 90-24 Upper mineralisation level*	Toe of Forbindelses gletscher Upper mineralisation levels	Drill core 90-23A Upper mineralisation level
Total number of grains		*208*	*932*		*1623*		*1092*	*626*
ML-2.2 (Au+1)								
Number of grains	*13*	*0*	*0*	*13*	*0*	*0*	*0*	*0*
Au and Ag minerals and phases		above	no data	**93.8***	*no data*	*above*	above	above
PGE with Sn, Bi, Pb, Te, Se, Sb		above	no data	-	*no data*	*above*	above	above
Arsenides		above	no data	**6.2***	*no data*	*above*	above	above
Sulfides		above	no data	-	*no data*	*above*	above	above
Intermetallic alloys		above	no data	-	*no data*	*above*	above	above
ML–2.1 (Pd1 and Pd1/Au)								
Number of grains	*585*	*0*	*0*	*206*	*228*	*41*	*0*	*0*
Au and Ag minerals and phases		above	no data	**23.4**	**36.3**	**98.5**	above	above
PGE with Sn, Bi, Pb, Te, Se, Sb		above	no data	0.9	1.1	0.2	above	above
Arsenides		above	no data	0.0	0.0	0.0	above	above
Sulfides		above	no data	0.0	0.6	1.4	above	above
Intermetallic alloys		above	no data	**75.6**	**61.9**	0.0	above	above
ML–2 (Pd2a and b)								
Number of grains	*438*	*0*	*152*	*144*	*47*	*95*	*0*	*0*
Au and Ag minerals and phases		above	**3.8**	**15.0**	**48.2**	**8.8**	above	above
PGE with Sn, Bi, Pb, Te, Se, Sb		above	1.0	4.7	1.0	0.7	above	above
Arsenides		above	0.0	**6.5**	0.0	0.0	above	above
Sulfides		above	0.2	**67.9**	2	**15.0**	above	above
Intermetallic alloys		above	**94.9**	**5.0**	**48.8**	**75.6**	above	above

Table 4 continued

ML–1.2 (Pd3a and b)								
Number of grains	*866*			*37*	*270*	*63*	*496*	
Au and Ag minerals and phases		above	no data	**17.3**	**0.9**	**1.9**	**84.7**	above
PGE with Sn, Bi, Pb, Te, Se, Sb		above	no data	**3.6**	**1.0**	**0.6**	0.4	above
Arsenides		above	no data	-	-	0.0	0.0	above
Sulfides		above	no data	**71.3**	**8.2**	0.0	0.0	above
Intermetallic alloys		above	no data	**8.4**	**89.8**	**97.5**	**14.9**	above
ML–1.1 (Pd4a and b)		Above level						
Number of grains	*482*	*89*		25	*78*	*122*		*179*
Au and Ag minerals and phases		**92.7**	no data	6.1	**0.7**	1.2	no data	**94.8**
PGE with Sn, Bi, Pb, Te, Se, Sb		0.9	no data	0.4	**0.7**	0.8	no data	0.4
Arsenides		5.5	no data	n.d.	-	0.0	no data	4.8
Sulfides		1.0	no data	**41.1**	**0.6**	**1.0**	no data	0.0
Intermetallic alloys		0.0	no data	**46.3**	**98.4**	**96.9**	no data	0.0
ML–0 (Pd5 and Pd6)								
Number of grains	*2196*	*119*		*368*	*33*	*666*	*596*	*447*
Au and Ag minerals and phases		**10.9**	no data	2.2	0.0	1.2	1.0	**15.5**
PGE with Sn, Bi, Pb, Te, Se, Sb		6.7	no data	1.8	0.6	1.2	0.4	**53.4**
Arsenides		**28.6**	no data	0.1	0.0	0.9	0.8	**24.7**
Sulfides		**53.6**	no data	**18.2**	0.1	0.0	3.0	4.3
Intermetallic alloys		0.4	no data	**78.0**	**99.3**	**96.4**	**94.8**	1.5

* Sample 90-22 977,

Table 5: Stratigraphic variation in relative importance of precious metal mineral groups in Pd5 in drill cores 90-23A and 90-10 from near the E and W margins, respectively. Each sample collects t a 1-metre intervat inn the drill core.

Mineral	General formula	90-23A samples				90-10 samples		
		808	807	806	avg.	445	443	avg.
Au, Ag and Pt phases		**1.9**	**8**	**36.3**	**15.4**	**0**	**21.7**	**10.8**
Au-phases		**1.9**	**8**	**28.3**	**12.7**	**0**	**21.7**	**10.8**
(Au,Cu,Pd,Ag) alloys	(Au,Cu,Pd,Ag,Pt)	0.7	8	23	10.6	0	17.3	8.65
Bogdanovite	$(Au,Pd,Pt)_3(Cu,Fe)$	1.2	n.d.	5	2.1	0	0	0
Tetra-auricupride	(Au,Pd,Pt)(Cu,Fe)	n.d.	n.d.	0.3	0.1	0	4.4	2.2
Ag-phases		**0**	**0**	**8**	**2.7**	**0**	**0**	**0**
Native silver	(Ag)	n.d.	0	n.d.	0	0	0	0
Polybasite	$[(Ag,Cu)_6(Sb,As)_2S_7][Ag9CuS_4]$	n.d.	0	n.d.	0	0	0	0
Stephanite	Ag_5SbS_4	n.d.	n.d.	8	2.7	0	0	0
Others								
Plumbides, tellu tellurides and stannides		**74.2**	**60**	**26.6**	**53.6**	**0**	**5.8**	**2.9**
Kotulskite	Pd(Te,Pb)	n.d.	n.d.	0.3	0.1	0	0	0
Keithconnite	$Pd_{3-x}(Te,Pb,As,Sn)$	0.5	2	2	1.5	0	4	0.2
Zvyagintsevite	$(Pd,Au,Pt)_3(Pb,Sn)$	73	58	24	51.7	0	1.8	0.9
Atokite	$(Pd,Pt)_3(Sn,As,Te)$	n.d.		0.3	0.1	0	0	0
Arsenides		**11.7**	**25**	**36.3**	**24.7**	**34.8**	**29.8**	**32.3**
Arsenopalladinite	$(Pd,Cu,Au)_8(As,Sn)_3$	3	11	17	10.3	0	0	0
Guanglinite	$(Pd,Cu,Au)_3(As,Sn,Te,Sb)$	8	12	8	9.3	30.3	24.8	27.6
Palladoarsenide	$(Pd,Cu)_2As$	0.7	2	2	1.6	0	0	0
Isomertieite	$Pd_{11}As_2(Sb,Te)_2$	0.7	n.d.	0.3	0.3	0	0	0
Sperrylite	$PtAs_2$	0.5	0	9	3.2	0	0	0
Atokite	$(Pd,Pt,Au)_3(Sn,Pb,As)$	0	0	0	0	2.6	5	3.8
Unnamed						1.9	0	0.95
Sulphides		**10**	**2**	**1**	**4.3**	**64.5**	**42.6**	**53.6**
Vysotskite	(Pd,Ni)S	4	0	n.d.	1.3	19.1	22.5	20.8
Vasilite	$Pd_{12}Cu_4S_7$	6	2	1	3	45.4	20.1	32.8
Pd and Pd-alloys		**1**	**3**	**0**	**1.3**	**0.7**	**0**	**0.4**
Native palladium	(Pd)	n.d.	3	n.d.	1	0	0	0
Skaergaardite	PdCu	1	n.d.	n.d.	0.3	0.7	0	0.4
Pt-alloy	(Pt,Pd,Fe,Cu)	0.7	0	n.d.	0.2	0	0	0

n.d.: No data

Table 6. Grade times width* for Pd, Pt and Au in Skaergaard PGE-Au Mineralisation

Drill core	from metres	to metres	Distance from western margin (see Nielsen et al., 2015)	Distance from center at at point 666 (m) (see text)	Pd	Pt	Au	Pd+Pt	Pd+Pt +Au	Pd/Pt	Au/Pd	Au/Pt	PGE % of all In core through deposit	Au % of all In core through deposit
Pd5, 5 meters of core with highest Pd+Pt **														
89-02	201.0	206.0	2490	1559	10.45	0.84	0.31	11.29	11.60	12.51	0.030	0.37	30.1	3.8
89-03	255.0	260.0	1460	1588	8.24	0.81	0.48	9.05	9.53	10.17	0.058	0.59	34.4	6.8
89-04	272.0	277.0	1475	1588	6.43	0.76	0.39	7.20	7.58	8.42	0.060	0.51	30.8	4.6
89-06	159.0	164.0	4500	2735	9.54	0.75	0.36	10.28	10.64	12.80	0.038	0.48	39.1	5.1
89-09	484.0	489.0	1800	1324	7.68	0.73	0.36	8.41	8.77	10.46	0.047	0.50	26.9	4.4
90-10	442.6	447.6	340	2500	11.98	0.64	0.78	12.62	13.40	18.70	0.065	1.21	55.5	19.4
90-11	675.1	680.1	1970	1382	6.97	0.64	0.39	7.61	8.00	10.95	0.056	0.62	23.5	4.3
90-13	469.0	474.0	1300	1706	7.08	0.65	0.33	7.73	8.06	10.84	0.047	0.51	24.9	3.3
90-14	192.9	198.0	400	2559	11.19	0.75	0.63	11.94	12.57	14.89	0.056	0.83	62.2	15.3
90-17A	498.0	503.0	740	2118	8.64	0.75	0.26	9.39	9.65	11.52	0.030	0.35	38.6	4.9
90-18	1009.0	1014.0	1200	1824	6.15	0.76	0.33	6.91	7.24	8.11	0.054	0.44	18.6	3.5
90-19	589.0	594.0	5270	1824	6.57	0.65	0.37	7.22	7.59	10.11	0.056	0.57	24.9	3.9
90-20	975.0	980.0	1860	2588	4.68	0.88	0.33	5.56	5.89	5.33	0.071	0.38	18.3	3.3
90-22	810.0	815.0	2690	1029	9.15	0.89	0.41	10.04	10.45	10.29	0.045	0.46	26.9	3.6
90-23A	806.0	811.0	6700	3441	9.30	0.62	0.61	9.92	10.53	15.00	0.066	0.99	47.5	15.8
90-24	1055.0	1060.0	3350	294	8.80	0.74	0.35	9.54	9.89	11.89	0.040	0.47	28.1	2.7
04-28A	471.0	475.3	5147	2273	8.10	0.82	0.41	8.92	9.33	9.86	0.051	0.50	26.5	4.7
04-30	1168.0	1173.0	1500	2000	5.50	0.73	0.53	6.23	6.76	7.53	0.096	0.73	55.4	14.9
04-31	1170.0	1176.0	2400	1357	8.71	0.65	0.42	9.36	9.79	13.31	0.049	0.65	35.2	4.3
04-32	412.0	417.0	1600	1500	13.61	0.7	0.59	14.31	14.90	19.44	0.043	0.84	21.5	5.4
04.33	411.0	416.0	4559	1714	7.62	0.67	0.45	8.29	8.74	11.37	0.059	0.67	24.9	3.4
04-34	460.0	465.0	5500	3286	9.22	0.76	0.71	9.98	10.69	12.13	0.077	0.93	42.4	5.1
11-53	475.0	480.0	1765	1549	8.37	0.83	0.48	9.20	9.68	10.08	0.057	0.58	27.6	4.8
11-57	114.0	119.0	6200	3803	10.77	0.73	1.09	11.50	12.59	14.75	0.101	1.50	36.6	8.2

Table 6 continued.....

LPGEM (Pd6-Pd4): from a lower cut-off of 100 ppb Pd+Pt to Pd+Pt low between Pd4a and Pd3b

89-02	191.0	218.0	2490	1559	22.52	2.29	1.01	24.80	25.81	9.83	0.045	0.44	66.1	12.2
89-03	245.0	267.0	1460	1588	16.31	1.88	1.27	18.19	19.46	8.69	0.078	0.67	69.2	18.0
89-04	258.0	283.0	1475	1588	15.34	1.71	1.59	17.05	18.64	8.97	0.103	0.93	73.1	19.1
89-06	144.0	173.0	4500	2735	22.16	2.14	2.03	24.30	26.32	10.37	0.092	0.95	92.4	28.9
89-09	473.0	495.6	1800	1324	16.68	1.76	0.81	18.44	19.25	9.45	0.049	0.46	59.0	9.8
90-10	429.0	457.6	340	2500	21.07	1.68	4.00	22.75	26.75	12.54	0.190	2.38	100.0	100.0
90-11	663.5	691.5	1970	1382	16.51	1.89	0.96	18.40	19.36	8.75	0.058	0.51	56.7	10.4
90-13	459.0	483.0	1300	1706	16.22	1.83	1.07	18.04	19.12	8.88	0.066	0.59	58.0	10.6
90-14	173.5	208.0	400	2559	17.57	1.63	4.09	19.19	23.28	10.80	0.233	2.51	100.0	100.0
90-17A	484.0	512.9	740	2118	19.50	1.92	1.08	21.42	22.49	10.18	0.055	0.56	88.1	19.9
90-18	998.3	1025.7	1200	1824	15.38	2.13	0.86	17.51	18.37	7.21	0.056	0.40	47.2	8.9
90-19	571.0	603.0	5270	1824	18.33	1.83	1.22	20.17	21.39	10.01	0.067	0.67	69.5	13.1
90-20	962.0	992.0	1860	2588	14.87	2.15	0.80	17.01	17.82	6.92	0.054	0.37	56.1	8.0
90-22	1020.0	1045.0	2690	1029	20.25	2.17	1.37	22.42	23.80	9.33	0.068	0.63	60.0	12.1
90-23A	794.0	822.0	6700	3441	19.12	1.74	3.90	20.87	24.76	10.98	0.204	2.24	100.0	100.0
90-24	1045.0	1070.0	3350	294	19.80	2.02	0.87	21.82	22.69	9.80	0.044	0.43	64.4	6.9
04-28A	461.0	484.0	5147	2273	15.90	1.46	0.90	17.36	18.26	10.91	0.056	0.62	60.2	12.5
04-30	1155.0	1175.9	1500	2000	10.37	1.30	0.90	11.67	12.57	7.95	0.087	0.69	96.7	72.6
04-31	1152.0	1184.5	2400	1357	23.29	2.10	2.02	25.39	27.69	11.06	0.099	1.09	68.5	9.5
04-32	399.0	425.0	1600	1500	26.89	1.50	2.50	28.39	30.89	17.93	0.093	1.67	45.1	9.2
04-33	396.0	425.0	4559	1714	19.35	1.90	1.63	21.25	22.88	10.21	0.084	0.86	67.6	18.4
04-34	450.0	477.0	5500	3286	19.10	2.09	1.70	21.19	22.89	9.14	0.089	0.81	92.9	71.7
11-53	465.0	490.0	1765	1549	18.79	2.11	1.28	20.90	22.18	8.91	0.068	0.61	70.6	17.6
11-57	98.0	127.0	6200	3803	18.20	1.87	5.35	20.07	25.41	9.76	0.294	2.87	77.6	19.6

Table 6 continued……

*Pd6 to Pd1/Au: Pd+Pt+Au from a lower to an upper cut-off of 100ppb Pd+Pt+Au****

89-02	163.0	218.0	2490	1559	34.45	3.06	8.25	37.51	45.76	11.26	0.239	2.70	100	100
89-03	230.0	267.0	1460	1588	24.00	2.30	7.03	26.30	33.33	10.42	0.293	3.05	100	100
89-04	251.2	283.0	1475	1588	21.19	2.15	8.31	23.34	31.64	9.85	0.392	3.86	100	100
89-06	138.0	173.0	4500	2735	24.00	2.30	7.03	26.30	33.33	10.42	0.293	3.05	100	100
89-09	444.8	495.6	1800	1324	28.87	2.41	8.04	31.28	39.32	11.97	0.279	3.34	100	100
90-10	429.0	457.6	340	2500	21.07	1.68	4.00	22.75	26.75	12.54	0.190	2.38	100	100
90-11	635.8	691.5	1970	1382	29.77	2.68	9.22	32.45	41.67	11.10	0.310	3.44	100	100
90-13	421.0	483.0	1300	1706	28.39	2.71	10.10	31.10	41.19	10.48	0.356	3.73	100	100
90-14	173.5	208.0	400	2559	17.57	1.63	4.09	19.19	23.28	10.80	0.233	2.51	100	100
90-17A	471.6	512.9	740	2118	22.13	2.17	5.41	24.30	29.71	10.18	0.244	2.49	100	100
90-18	946.0	1025.7	1200	1824	33.82	3.30	9.61	37.12	46.72	10.25	0.284	2.91	100	100
90-19	551.0	603.0	5270	1824	26.62	2.40	9.33	29.02	38.35	11.12	0.351	3.90	100	100
90-20	935.0	992.0	1860	2588	27.40	2.93	10.04	30.32	40.37	9.36	0.367	3.43	100	100
90-22	978.0	1045.0	2690	1029	34.21	3.16	11.34	37.37	48.71	10.82	0.331	3.59	100	100
90-23A	794.0	822.0	6700	3441	19.12	1.74	3.90	20.87	24.76	10.98	0.204	2.24	100	100
90-24	1018.0	1070.0	3350	294	31.15	2.75	12.67	33.89	46.56	11.34	0.407	4.61	100	100
04-28A	436.0	484.0	5147	2273	23.31	2.04	9.44	25.34	34.79	11.45	0.405	4.64	100	100
04-30	1121.0	1175.9	1500	2000	26.72	2.31	9.79	29.03	38.81	11.57	0.366	4.24	100	100
04-31	1110.0	1184.5	2400	1357	34.78	2.80	12.48	37.58	50.06	12.40	0.359	4.45	100	100
04-32	371.0	425.0	1600	1500	32.00	2.02	11.46	34.02	45.48	15.84	0.358	5.67	100	100
04-33	377.0	425.0	4559	1714	27.69	2.40	9.29	30.09	39.38	11.56	0.335	3.88	100	100
04-34	419.0	477.0	5500	3286	24.61	2.68	8.67	27.29	35.96	9.18	0.352	3.24	100	100
11-53	433.0	490.0	1765	1549	31.76	2.95	10.25	34.71	44.96	10.77	0.323	3.47	100	100
11-57	89.0	127.0	6200	3803	18.52	2.22	7.36	20.74	28.10	8.34	0.397	3.32	100	100

*Grade times width (g*w) is the average grade over a given stratigraphic interval in grams/ton multiplied by its height in metres.
**Exception: Drill core 04-28A from which the lower part of Pd5 is missing and core 31 in which Pd5 is cut by a dike.
***With the exception of 90-18 that has an Au concentration in Au+1 elevated ~ 12 meters above the Au/Pd1. See text for further information.

Table 7. Bulk rock ((Pd+Pt+Au)/Cu)*1000 ratios in Pd5 relative to peak concentration (1-m averages)

Drill core	PRL 11-57	PRL08-35A*	90-23A*	SKM 04-34	90-14*	SKM 04-30	90-18*	90-22**	SKM 04-32	PRL11-53	SKM 04-28A	SKM 04-31	SKM 04-33	90-24*
	East margin				West margin		SW sector		Central part of intrusion					
Depth (m) relative to Pd5 peak	((Pd+Pt+Au)/Cu) * 1000													
4.0	3.77	3.10	1.74	2.71	-	9.17	-	2.17	4.69	4.98	4.61	6.76	7.02	-
3.0	3.66	6.30	-	1.71	-	7.84	-	3.22	7.26	8.32	5.35	11.9	6.72	-
2.0	7.58	11.00	-	4.55	-	7.47	-	7.93	12.70	15.35	9.61	8.79	10.62	-
1.0	12.33	15.00	10.48	11.10	-	11.30	-	13.54	21.26	20.63	20.43	23.52	21.36	-
0.0	13.33	16.00	-	17.21	14.29	16.11	18.15	16.53	19.35	20.62	22.09	25.15	27.67	29.49
-1.0	11.36	12.40	-	14.89	-	13.33	-	15.90	18.24	16.61	14.48	15.82	19.72	-
-2.0	6.94	8.50	8.69	13.61	-	8.83	-	9.10	18.22	11.67	10.29	11.91	13.26	-
-3.0	7.18	6.70	6.67	7.33	-	6.53	-	7.97	14.82	8.96	7.50	9.09	10.52	-
-4.0	6.69	-	-	5.15	-	7.36	-	5.79	10.64	7.61	8.66	8.41	8.66	-
-5.0	6.55	-	-	5.16	-	7.04	-	4.86	7.87	9.87	7.51	8.70	8.88	-
-6.0	6.30	-	-	4.96	-	-	-	4.58	6.14	8.55	7.67	8.76	1.46	-
-7.0	5.65	-	-	4.53	-	-	-	3.22	6.17	10.59	6.67	9.24	10.38	-
-8.0	3.48	-	-	5.00	-	-	-	5.08	5.51	8.75	4.54	6.94	8.33	-

* No systematic Cu determinations. Cu values from samples collected at intervals (J.C.Ø Andersen, unpublished).

**All data are based on 1-m averages and are +/- 0.5 m in elevation. In Fig. 10 the data for 90-22 have been moved up 0.5 m to align the Pd5 peak.

Table 8: Summary of the first six principal components from the PCA

Principal component	PC1	PC2	PC3	PC4	PC5	PC6
Eigenvalues	6.26	3.68	1.32	0.76	0.63	0.46
Proportion of total variance (%)	44.75	26.30	9.40	5.44	4.56	3.28
Cumulative proportion of total variance (%)	44.75	71.05	80.45	85.89	90.46	93.73
Eigenvectors (loadings)						
Ti	0.19	-0.39	-0.08	0.06	-0.48	0.14
Fe3+	0.18	-0.38	0.19	-0.18	-0.07	-0.08
P	0.14	0.32	-0.43	0.07	-0.44	-0.28
Pd	-0.35	-0.11	-0.28	-0.14	0.01	0.10
Pt	-0.34	-0.06	-0.15	0.44	0.24	-0.05
Au	-0.19	0.21	0.48	-0.59	-0.22	-0.06
V	0.11	-0.46	-0.06	-0.07	0.29	0.04
Cu	0.22	0.00	0.54	0.49	-0.02	-0.46
Zn	0.26	-0.38	-0.06	-0.16	0.06	0.02
Y	0.34	0.09	-0.08	-0.17	0.46	-0.17
Zr	0.36	-0.03	-0.12	0.10	-0.31	0.11
Ce	0.30	0.26	-0.18	-0.13	0.11	-0.02
Nd	0.35	0.21	-0.14	-0.15	0.23	-0.08
Pb	0.23	0.26	0.25	0.22	0.07	0.79

Details of analysis and method in text and EA14